

Pushing coarse-grained models beyond the continuum limit using equation learning

Daniel J. VandenHeuvel¹, Pascal R. Buenzli¹, and Matthew J. Simpson^{1, *}

¹School of Mathematical Sciences, Queensland University of Technology, Brisbane, Australia.

*Corresponding author: matthew.simpson@qut.edu.au

December 20, 2023

Abstract

Mathematical modelling of biological population dynamics often involves proposing high fidelity discrete agent-based models that capture stochasticity and individual-level processes. These models are often considered in conjunction with an approximate coarse-grained differential equation that captures population-level features only. These coarse-grained models are only accurate in certain asymptotic parameter regimes, such as enforcing that the time scale of individual motility far exceeds the time scale of birth/death processes. When these coarse-grained models are accurate, the discrete model still abides by conservation laws at the microscopic level, which implies that there is some macroscopic conservation law that can describe the macroscopic dynamics. In this work, we introduce an equation learning framework to find accurate coarse-grained models when standard continuum limit approaches are inaccurate. We demonstrate our approach using a discrete mechanical model of epithelial tissues, considering a series of four case studies that consider problems with and without free boundaries, and with and without proliferation, illustrating how we can learn macroscopic equations describing mechanical relaxation, cell proliferation, and the equation governing the dynamics of the free boundary of the tissue. While our presentation focuses on this biological application, our approach is more broadly applicable across a range of scenarios where discrete models are approximated by approximate continuum-limit descriptions. All code and data to reproduce this work are available at <https://github.com/DanielVandH/StepwiseEQL.jl>.

1 Introduction

Mathematical models of population dynamics are often constructed by considering both discrete and continuous descriptions, allowing for both microscopic and macroscopic details to be considered [1]. This approach has been applied to several kinds of discrete models, including cellular Potts models [2–5], exclusion processes [6–9], mechanical models of epithelial tissues [10–17], hydrodynamics [18, 19], and a variety of other types of individual-based models [1, 20–27]. Continuum models are useful for describing collective behaviour, especially because the computational requirement of discrete models increases with the size of the population, and this can become computationally prohibitive for large populations, which is particularly problematic for parameter inference [28]. In contrast, the computational requirement to solve a continuous model is independent of the population size, and generally requires less computational overhead than working with a discrete approach only [15]. Continuum models are typically obtained by coarse-graining the discrete model, using Taylor series expansions to obtain continuous partial differential equation (PDE) models that govern the population densities on a continuum or macroscopic scale [10, 11, 29, 30].

One challenge with using coarse-grained continuum limit models is that while the solution of these models can match averaged data from the corresponding discrete model for certain choices of parameters

[10, 17, 31], the solution of the continuous model can be a very poor approximation for other parameter choices [13, 15, 32, 33]. More generally, coarse-grained models are typically only valid in certain asymptotic parameter regimes [31, 33, 34]. For example, suppose we have a discrete space, discrete time, agent-based model that incorporates random motion and random proliferation. Random motion involves stepping a distance Δ with probability $P_m \in [0, 1]$ per time step of duration τ . The stochastic proliferation process involves undergoing proliferation with probability $P_p \in [0, 1]$ per unit time step. The continuum limit description of this kind of discrete process can be written as [33]

$$\frac{\partial q}{\partial t} = \frac{\partial}{\partial x} \left(D(q) \frac{\partial q}{\partial x} \right) + R(q), \quad (1)$$

where q is the macroscopic density of individuals, $D(q)$ is the nonlinear diffusivity that describes the effects of individual migration, and $R(q)$ is a source term that describes the effects of the birth process in the discrete model [33]. Standard approaches to derive (1) require $D(q) = \mathcal{O}(P_m \Delta^2 / \tau)$ and $R(q) = \mathcal{O}(P_p / \tau)$ in the limit that $\Delta \rightarrow 0$ and $\tau \rightarrow 0$. To obtain a well-defined continuum limit such that the diffusion and source terms are both present in the macroscopic model, some restrictions on the parameters in the discrete model are required [33, 34]. Typically, this is achieved by taking the limit as $\Delta \rightarrow 0$ and $\tau \rightarrow 0$ jointly such that the ratio Δ^2 / τ remains finite, implying that $P_p = \mathcal{O}(\tau)$ so that both the diffusion and source terms in (1) are $\mathcal{O}(1)$. In practice, this means that the time scale of individual migration events has to be much faster than the time scale of individual proliferation events, otherwise the continuum limit description is not well defined [33, 34]. If this restriction is not enforced, then the solution of the continuum limit model does not always predict the averaged behaviour of the discrete model [33], as the terms on the right-hand side of (1) are no longer $\mathcal{O}(1)$ so that the continuum limit is not well defined [34].

Regardless of whether choices of parameters in a discrete model obey the asymptotic restrictions imposed by coarse-graining, the discrete model still obeys a conservation principle, which implies that there is some alternative macroscopic conservation description that will describe population-level features of interest [35, 36]. Equation learning is a means of determining appropriate continuum models outside of the usual continuum limit asymptotic regimes. Equation learning has been used in several applications for model discovery. In the context of PDEs, a typical approach is to write $\partial q / \partial t = \mathcal{N}(q, \mathcal{D}, \theta)$, where q is the population density, \mathcal{N} is some nonlinear function parametrised by θ , \mathcal{D} is a collection of differential operators, and θ are parameters to be estimated [37]. This formulation was first introduced by Rudy et al. [37], who extended previous work in learning ordinary differential equations (ODEs) proposed by Brunton et al. [38]. Equation learning methods developed for the purpose of learning biological models has also been a key interest [39, 40]. Lagergren et al. [41] introduce a biologically-informed neural network framework that uses equation learning that is guided by biological constraints, imposing a specific conservation PDE rather than a general nonlinear function \mathcal{N} . Lagergren et al. [41] use this framework to discover a model describing data from simple *in vitro* experiments that describe the invasion of populations of motile and proliferative prostate cancer cells. VandenHeuvel et al. [42] extend the work of Lagergren et al. [41], incorporating uncertainty quantification into the equation learning procedure through a bootstrapping approach. Nardini et al. [32] use discrete data from agent-based models to learn associated continuum ODE models, combining a user-provided library of functions together with sparse regression methods to give simple ODE models describing population densities. Regression methods have also been used as an alternative to equation learning for this purpose [43].

These previous approaches to equation learning consider various methods to estimate the parameters θ , such as sparse regression or nonlinear optimisation [32, 37–39, 41, 42], representing \mathcal{N} as a library of functions [37–39], neural networks [41], or in the form of a conservation law with individual components to be learned [41, 42]. In this work, we introduce a *stepwise equation learning* framework, inspired from stepwise regression [44], for estimating θ from averaged discrete data with a given \mathcal{N} representing a proposed form for the continuum model description. We incorporate or remove terms one at a time until a parsimonious continuum model is obtained whose solution matches the data well and no further improvements can be made to this match. Our approach is advantageous for several reasons. Firstly, it is computationally efficient and parallelisable, allowing for rapid exploration of results with different discrete parameters and different forms of \mathcal{N} for a given data set. Secondly, the approach is modular, with different mechanistic features easily

incorporated. This approach enables extensive computational experimentation by exploring the impact of including or excluding putative terms in the continuum model without any great increase in computational overhead. Lastly, it is easy to examine the results from our procedure, allowing for ease of diagnosing and correcting reasons for obtaining poor fitting models, and explaining what components of the continuum model are the most influential. We emphasise that a key difference between our approach and other work, such as the methods developed by Brunton et al. [38] and Rudy et al. [37], is that we constrain our problem so that we can only learn conservation laws rather than allow a general form through a library of functions, and that we iteratively eliminate variables from θ rather than use sparse regression. These important features are what support the modularity and interpretability of our approach.

To illustrate our procedure, we consider a discrete, individual-based one-dimensional toy model inspired from epithelial tissues [10, 17]. Epithelial tissues are biological tissue composed of cells, organised in a monolayer, and are present in many parts of the body and interact with other cells [45], lining surfaces such as the skin and the intestine [46]. They are important in a variety of contexts, such as wound healing [47, 48] and cancer [49, 50]. Many models have been developed for studying their dynamics, considering both discrete and continuum modelling [10–16], with most models given in the form of a nonlinear reaction-diffusion equation with a moving boundary, using a nonlinear diffusivity term to incorporate mechanical relaxation and a source term to model cell proliferation [12, 13, 16]. These continuum limit models too are only accurate in certain parameter regimes, becoming inaccurate if the rate of mechanical relaxation is slow relative to the rate of proliferation [13, 15, 33]. To apply our stepwise equation learning procedure, we let the nonlinear function \mathcal{N} be given in the form of a conservation law together with equations describing the free boundary. We demonstrate this approach using a series of four biologically-motivated case studies, considering problems with and without a free boundary, and with and without proliferation, with each case study building on those before it. The first two case studies are used to demonstrate how our approach can learn known continuum limits, while the latter two case studies show how we can learn improved continuum limit models in parameter regimes where these known continuum limits are no longer accurate. We implement our approach in the JULIA language [51], and all code is available on GitHub at <https://github.com/DanielVandH/StepwiseEQL.jl>.

2 Mathematical model

Following Murray et al. and Baker et al. [10, 16], we suppose that we have a set of nodes $x_1, \dots, x_n(t)$ describing n cell boundaries at a time t . The interval $(x_i(t), x_{i+1}(t))$ represents the i th cell for $i = 1, \dots, n-1$, where we fix $x_1 = 0$ and $x_1 < x_2(t) < \dots < x_n(t)$. The number of nodes, n , may increase over time due to cell proliferation. We model the mechanical interaction between cells by treating them as springs, as indicated in Figure 1, so that each node i experiences forces $F_{i,i\pm 1}$ from nodes $i \pm 1$, respectively, except at the boundaries where there is only one neighbouring force. We further assume that each of these springs has the same mechanical properties, and that the viscous force from the surrounding medium is given by $\eta dx_i(t)/dt$ with drag coefficient η . Lastly, assuming we are in a viscous medium so that the motion is overdamped, we can model the dynamics of each individual node $x_i(t)$, fixing $x_1 = 0$, by [16]

$$\eta \frac{dx_i(t)}{dt} = F_{i,i-1} + F_{i,i+1}, \quad i = 1, \dots, n-1, \quad (2)$$

$$\eta \frac{dx_n(t)}{dt} = F_{n,n-1}, \quad (3)$$

where

$$F_{i,i\pm 1} = F(|x_i(t) - x_{i\pm 1}(t)|) \frac{x_i(t) - x_{i\pm 1}(t)}{|x_i(t) - x_{i\pm 1}(t)|} \quad (4)$$

is the interaction force that the i th node experiences from nodes $i \pm 1$ (Figure 1). In Case Studies 1 and 3 (see Section 3, below), we hold $x_n(t) = L$ constant and discard (3). Throughout this work, we use linear Hookean springs so that $F(\ell_i) = k(s - \ell_i)$, $\ell_i > 0$, where $\ell_i(t) = x_{i+1}(t) - x_i(t)$ is the length of the i th cell, $k > 0$ is the spring constant, and $s \geq 0$ is the resting spring length [10]; we discuss other force laws in Appendix E.

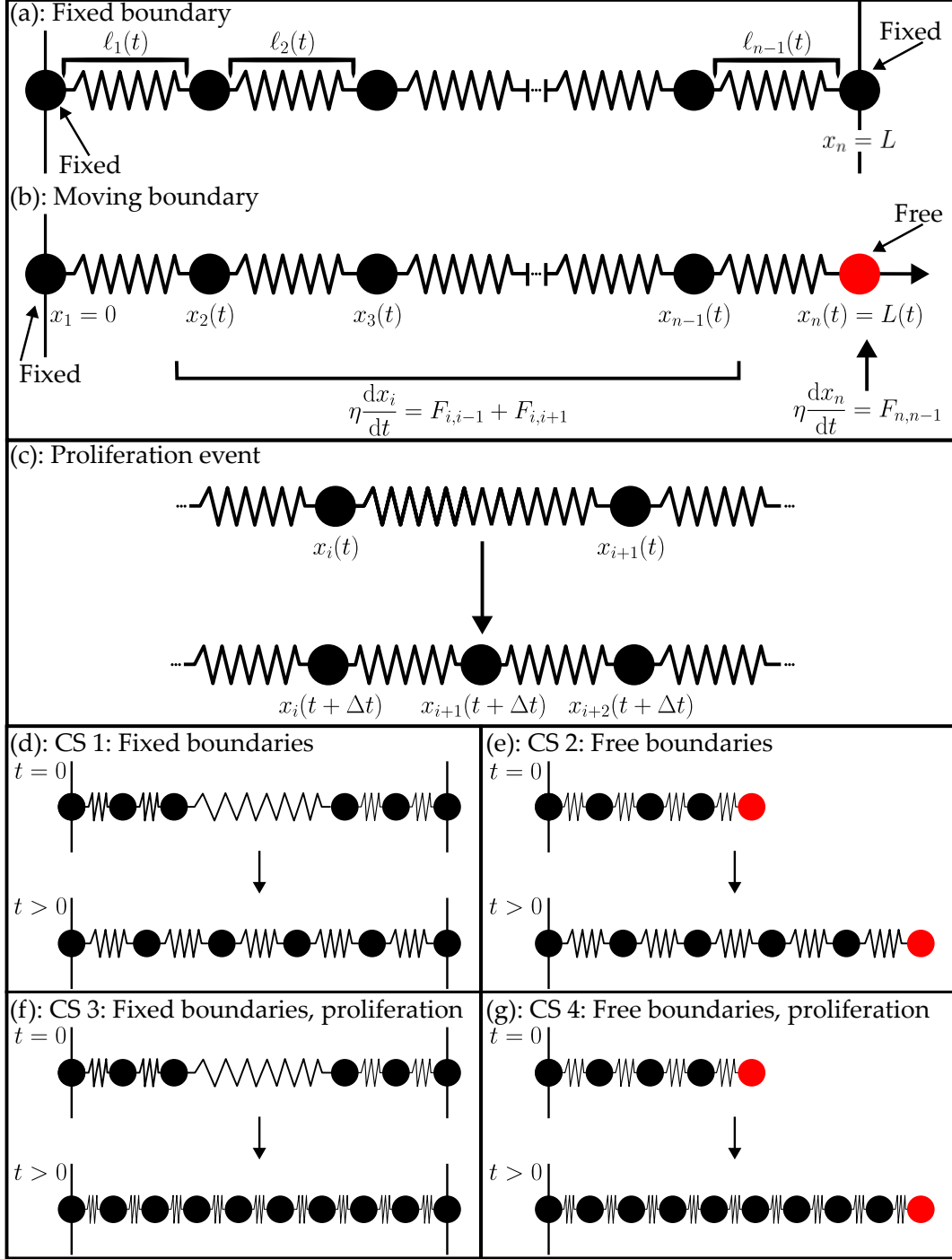


Figure 1: Discrete model and schematics for each case study (CS). (a) A fixed boundary problem with $x_1 = 0$ and $x_n = L$ fixed. (b) A free boundary problem with $x_1 = 0$ and $x_n(t) = L(t)$, shown in red, free. (c) Proliferation schematic, showing a cell $(x_i(t), x_{i+1}(t))$ dividing into $(x_i(t + \Delta t), x_{i+1}(t + \Delta t))$ and $(x_{i+1}(t + \Delta t), x_{i+2}(t + \Delta t))$ following a proliferation event, where $x_{i+1}(t + \Delta t) = (x_i(t) + x_{i+1}(t))/2$. (d)–(g) show schematics for the four case studies considered in the paper, where the first row in each panel is a representation of the initial configuration of cells at $t = 0$ and the second row a representation at a later time $t > 0$.

The dynamics governed by (2)–(3) describe a system in which cells mechanically relax. Following previous work [10,14,16], we introduce a stochastic mechanism that allows the cells to undergo proliferation, assuming only one cell can divide at a time over a given interval $[t, t + \Delta t)$ for some small duration Δt . We let the probability that the i th cell proliferates be given by $G_i \Delta t$, where $G_i = G(\ell_i)$ for some length-dependent proliferation law $G(\ell_i) > 0$. As represented in Figure 1(c), when the i th cell proliferates, the cell divides into two equally-sized daughter cells, and the boundary between the new daughter cells is placed at the midpoint of the original cell. Throughout this work, we use a logistic proliferation law $G(\ell_i) = \beta[1 - 1/(K\ell_i)]$ with $\ell_i > 1/K$, where β is the intrinsic proliferation rate and K is the carrying capacity density; we consider other proliferation laws in Appendix E. The implementation of the solution to these equations (2)–(3) and the proliferation mechanism is given in the JULIA package `EpithelialDynamics1D.jl`; in this implementation, if $G(\ell_i) < 0$ we set $G(\ell_i) = 0$ to be consistent with the fact that we interpret $G(\ell_i)$ as a probability. We emphasise that, without proliferation, we need only solve (2)–(3) once for a given initial condition in order to obtain the expected behaviour of the discrete model, because the discrete model is deterministic in the absence of proliferation. In contrast, incorporating proliferation means that we need to consider several identically-prepared realisations of the same stochastic discrete model to estimate the expected behaviour of the discrete model for a given initial condition.

In practice, macroscopic models of populations of cells are described in terms of cell densities rather than keeping track of the position of individual cell boundaries. The density of the i th cell $(x_i(t), x_{i+1}(t))$ is $1/\ell_i(t)$. For an interior node $x_i(t)$, we obtain a density $q_i(t)$ by taking the inverse of the average of the cells left and right of $x_i(t)$, giving

$$q_i(t) = \frac{2}{x_{i+1}(t) - x_{i-1}(t)}, \quad i = 2, \dots, n-1, \quad (5)$$

as in Baker et al. [16]. At boundary nodes, we use

$$q_1(t) = \frac{2}{x_2(t)} - \frac{2}{x_3(t)}, \quad q_n(t) = \frac{2}{x_n(t) - x_{n-1}(t)} - \frac{2}{x_n(t) - x_{n-2}(t)}, \quad (6)$$

derived by linear extrapolation of (5) to the boundary. The densities in (6) ensure that the slope of the density curves at the boundaries, $\partial q/\partial x$, match those in the continuum limit. We discuss the derivation of (6) in Appendix B. In the continuum limit where the number of cells is large and mechanical relaxation is fast, the densities evolve according to the moving boundary problem [10,16]

$$\begin{aligned} \frac{\partial q}{\partial t} &= \frac{\partial}{\partial x} \left(D(q) \frac{\partial q}{\partial x} \right) + R(q) & 0 < x < L(t), t > 0, \\ \frac{\partial q}{\partial x} &= 0 & x = 0, t > 0, \\ \frac{\partial q}{\partial x} &= H(q) & x = L(t), t > 0, \\ q \frac{dL}{dt} &= -D(q) \frac{\partial q}{\partial x} & x = L(t), t > 0, \end{aligned} \quad (7)$$

where $q(x, t)$ is the density at position x and time t , $D(q) = -1/(\eta q^2)F'(1/q)$, $R(q) = qG(1/q)$, $H(q) = -2qF(1/q)/[\eta D(q)]$, and $L(t) = x_n(t)$ is the leading edge position with $L(0) = x_n(0)$. The quantity $1/q$ in these equations can be interpreted as a continuous function related to the length of the individual cells. The initial condition $q(x, 0) = q_0(x)$ is a linear interpolant of the discrete densities $q_i(t)$ of the cells at $t = 0$. Similar to the discussion of (1), for this continuum limit to be valid so that both $D(q)$ and $R(q)$ play a role in the continuum model, constraints must be imposed on the discrete parameters. As discussed by Murphy et al. [15], we require that the time scale of mechanical relaxation is sufficiently fast relative to the time scale of proliferation. In practice this means that for a given choice of β we must have k/η sufficiently large for the solution of the continuum model to match averaged data from the discrete model. We note that, with our choices of F and G , the functions in (7) are given by

$$D(q) = \frac{k}{\eta q^2}, \quad R(q) = \beta q \left(1 - \frac{q}{K} \right), \quad H(q) = 2q^2(1 - qs). \quad (8)$$

For fixed boundary problems we take $H(q) = 0$ and $dL/dt = 0$. In [Appendix C](#), we describe how to solve (7) numerically, as well as how to solve the corresponding problem with fixed boundaries numerically.

3 Continuum-discrete comparison

We now consider four biologically-motivated case studies to illustrate the performance of the continuum limit description (7). These case studies are represented schematically in Figure 1(d)–(g). Case Studies 1 and 3, shown in Figure 1(d) and Figure 1(f), are fixed boundary problems, where we see cells relax mechanically towards a steady state where each cell has equal length. Case Studies 2 and 4 are free boundary problems, where the right-most cell boundary moves in the positive x -direction while all cells relax towards a steady state where the length of each cell is given by resting spring length s . Case Studies 1 and 2 have $\beta = 0$ so that there is no cell proliferation and the number of cells remains fixed during the simulations, whereas Case Studies 3 and 4 have $\beta > 0$ so that the number of cells increases during the discrete simulations. To explore these problems, we first consider cases where the continuum limit model is accurate, using the data shown in Figure 2, where we show space-time diagrams and a set of averaged density profiles for each problem in the left and right columns of Figure 2, respectively. Case Studies 1 and 3 initially place 30 nodes in $0 \leq x \leq 5$ and 30 nodes in $25 \leq x \leq 30$, or equivalently $n = 60$ with 28 cells in $0 \leq x \leq 5$ and 28 cells in $25 \leq x \leq 30$, spacing the nodes uniformly within each subinterval. Case Studies 2 and 4 initially place 60 equally spaced nodes in $0 \leq x \leq 5$.

The problems shown in Figure 2 use parameter values such that the solution of the continuum limit (7) is a good match to the averaged discrete density profiles. In particular, all problems use $k = 50$, $\eta = 1$, $s = 1/5$ and, for Case Studies 3 and 4, $\Delta t = 10^{-2}$, $K = 15$, and $\beta = 0.15$. The accuracy of the continuum limit is clearly evident in the right column of Figure 2 where, in each case, the solution of the continuum limit model is visually indistinguishable from averaged data from the discrete model. With proliferation, however, the continuum limit can be accurate when k/η is not too much larger than β , and we use Case Studies 3 and 4 to explore this.

Figure 3 shows further continuum-discrete comparisons for Case Studies 3 and 4 where we have slowed the mechanical relaxation by taking $k = 1/5$. This choice of k means that $D(q)$ and $R(q)$ are no longer on the same scale and thus the continuum limit is no longer well defined, as explained in the discussion of (1), meaning the continuum limit solutions are no longer accurate. In both cases, the solution of the continuum limit model lags behind the averaged data from the discrete model. In [Appendix A](#), we show the 95% confidence regions for each curve in Figure 3, where we find that the solutions have much greater variance compared to the corresponding curves in Figure 2 where $k = 50$.

We are interested in developing an equation learning method for learning an improved continuum model for problems like those in Figure 3, allowing us to extend beyond the parameter regime where the continuum limit (7) is accurate. We demonstrate this in Case Studies 1–4 in Section 4 where we develop such a method.

4 Learning accurate continuum limit models

In this section we introduce our method for equation learning and demonstrate the method using the four case studies from Figures 1–3. Since the equation learning procedure is modular, adding these components into an existing problem is straightforward. All JULIA code to reproduce these results is available at <https://github.com/DanielVandH/StepwiseEQL.jl>. A summary of all the parameters used for each case study is given in Table 1.

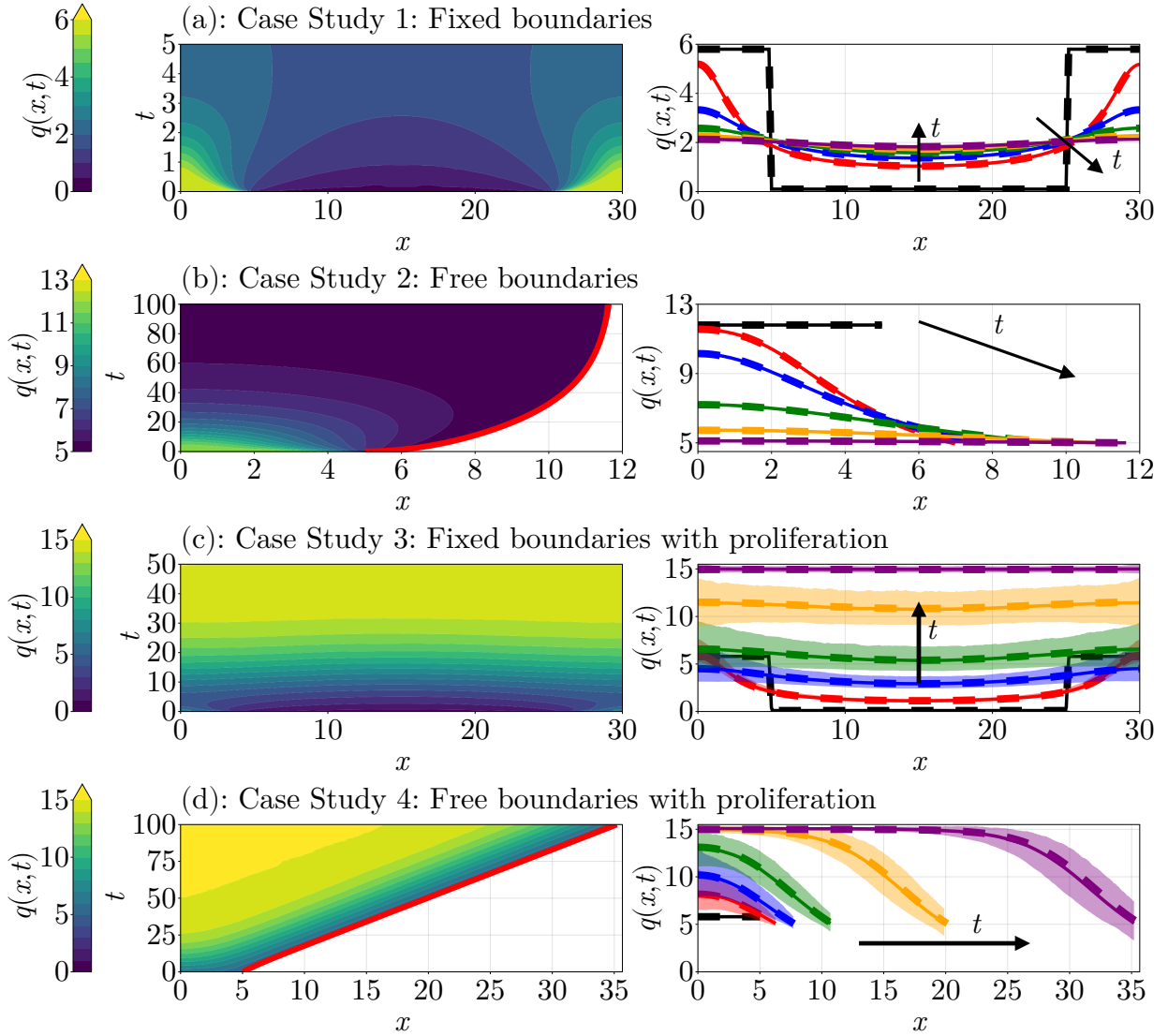


Figure 2: Space-time diagrams (left column) and densities (right column) for the four case studies from Figure 1 considered throughout the paper. The left column shows the evolution of the discrete densities in space and time, with (c) and (d) showing averaged results over 2500 identically-prepared realisations of the discrete model. In (b) and (d), the red line shows the position of the free boundary. In the figures in the right column, the solid curves are the discrete densities (5) and the dashed curves are solutions to the continuum limit problem (7), and the curves are given by black, red, blue, green, orange, and purple in the order of increasing time as indicated by the black arrows. The times shown are (a) $t = 0, 1, 2, 3, 4, 5$; (b) $t = 0, 5, 10, 25, 50, 100$; (c) $t = 0, 1, 5, 10, 20, 50$; and (d) $t = 0, 5, 10, 20, 50, 100$. In (c) and (d), the shaded regions show 95% confidence bands from the mean discrete curves at each time; the curves in (a) and (b) show no shaded regions as these models have no stochasticity.

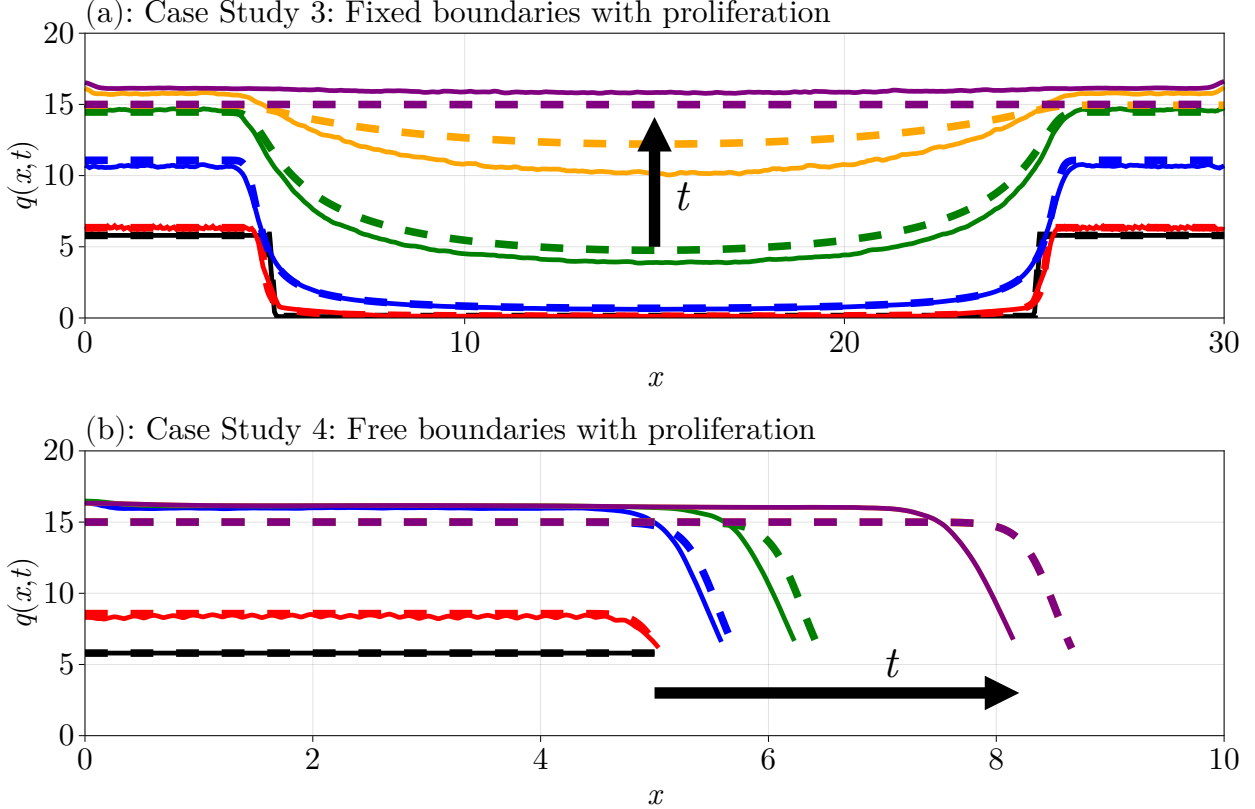


Figure 3: Examples of inaccurate continuum limits for (a) Case Study 3 and (b) Case Study 4, where both case studies use the same parameters as in Figure 2 except with $k = 1/5$ rather than $k = 50$. The solid curves are the discrete densities (5) and the dashed curves are solutions to the continuum limit problem (7). The arrows show the direction of increasing time. The density profiles are plotted in black, red, blue, green, orange, and purple for the respective times (a) $t = 0, 1, 10, 25, 40, 75$ and (b) $t = 0, 5, 25, 50, 100, 250$.

4.1 Case Study 1: Fixed boundaries

Case Study 1 involves mechanical relaxation only so that there is no cell proliferation and the boundaries are fixed, implying $R(q) = 0$ and $H(q) = 0$ in (7), respectively, and the only function to learn is $D(q)$.

Our equation learning approach starts by assuming that $D(q)$ is a linear combination of d basis coefficients $\{\theta_1, \dots, \theta_d\}$ and d basis functions $\{\varphi_1, \dots, \varphi_d\}$, meaning $D(q)$ can be represented as

$$D(q) = \sum_{i=1}^d \theta_i \varphi_i(q). \quad (9)$$

These basis functions could be any univariate function of q , for example the basis could be $\{\varphi_1, \varphi_2, \varphi_3\} = \{1/q, 1/q^2, 1/q^3\}$ with $d = 3$. In this work, we impose the constraint that $D(q) \geq 0$ for $q_{\min} \leq q \leq q_{\max}$, where q_{\min} and q_{\max} are the minimum and maximum densities observed in the discrete simulations, respectively. This constraint enforces the condition that the nonlinear diffusivity function is positive over the density interval of interest. While it is possible to work with some choices of nonlinear diffusivity functions for which $D(q) < 0$ for some interval of density [52–54], we wish to avoid the possibility of having negative nonlinear diffusivity functions and our results support this approach.

The aim is to estimate $\boldsymbol{\theta} = (\theta_1, \dots, \theta_d)^\top$ in (9). We use ideas similar to the basis function approach from VandenHeuvel et al. [42], using (9) to construct a matrix problem for $\boldsymbol{\theta}$. In particular, let us take the PDE

Parameter	Case Study						
	1	2	3a	3b	4a	4b	
k	50	50	50	1/5	50	1/5	
η	1	1	1	1	1	1	
s	1/5	1/5	1/5	1/5	1/5	1/5	
Δt	—	—	10^{-2}	10^{-2}	10^{-2}	10^{-2}	
β	—	—	0.15	0.15	0.15	0.15	
K	—	—	15	15	15	15	
M	50	150	501	751	(25, 50, 100, 250)	(20, 200, 200, 200)	
t_1	0	0	0	0	(0, 0, 5, 10)	(0, 2, 10, 20)	
t_M	5	15	50	75	(10^{-1} , 5, 10, 50)	(2, 10, 20, 50)	
n_s	—	—	1000	1000	1000	1000	
n_k	—	—	50	200	(25, 50, 100, 50)	(50, 100, 100, 100)	
τ_q	0.1	0.35	0.1	0.25	(0.1, 0, 0, 0)	(0, 0, 0, 0.3)	
$\tau_{dL/dt}$	—	0.1	—	—	(0, 0.2, 0, 0)	(0, 0.4, 0, 0)	
τ_t	0	0	0	0	0	(0.4, 0.4, 0, 0)	

Table 1: Parameters used for each case study. The parameters are k , the spring constant; η , the drag coefficient; s , the resting spring length; Δt , the proliferation duration; β , the intrinsic proliferation rate; K , the carrying capacity density; M , the number of time points; t_1 , the initial time; t_M , the final time; n_s , the number of identically-prepared realisations; n_k , the number of knots used for averaging over realisations; τ_q , which defines the $100\tau_q\%$ and $100(1 - \tau_q)\%$ density quantiles; $\tau_{dL/dt}$, which defines the $100\tau_{dL/dt}\%$ and $100(1 - \tau_{dL/dt})\%$ velocity quantiles; and τ_t , which defines the $100\tau_t\%$ and $100(1 - \tau_t)\%$ temporal quantiles. Values indicated by a line are not relevant for the corresponding case study. For Case Study 3 and 4, the label “a” refers to the accurate continuum limit case, and “b” refers to the inaccurate continuum limit case. For Case Study 4, some parameters are given by a set of four parameters, with the i th value of this set referring to the value used when learning the i th mechanism; see Section 44.4 for details.

(7), with $R(q) = 0$ and $H(q) = 0$, and expand the spatial derivative term so that we can isolate the θ_k terms,

$$\frac{\partial q_{ij}}{\partial t} = \sum_{k=1}^d \left\{ \frac{d\varphi_k(q_{ij})}{dq} \left(\frac{\partial q_{ij}}{\partial x} \right)^2 + \varphi_k(q_{ij}) \frac{\partial^2 q_{ij}}{\partial x^2} \right\} \theta_k, \quad (10)$$

where we let q_{ij} denote the discrete density at position $x_{ij} = x_i(t_j)$ and time t_j . We note that while q_{ij} is discrete, we assume it can be approximated by a smooth function, allowing us to define these derivatives $\partial q_{ij}/\partial t$, $\partial q_{ij}/\partial x$, and $\partial^2 q_{ij}/\partial x^2$ in (10); this assumption is appropriate since, as shown in Figure 2, these discrete densities can be well approximated by smooth functions. These derivatives are estimated using finite differences, as described in Appendix D. We also emphasise that, while (10) appears similar to results in [37, 38], the crucial difference is that we are specifying forms for the *mechanisms* of the PDE rather than the *complete* PDE itself; one other important difference is in how we estimate θ , defined below and in (15). We save the solution to the discrete problems (2)–(3) at M times $0 = t_1 < t_2 < \dots < t_M$ so that $i \in \{1, \dots, n\}$ and $j \in \{2, \dots, M\}$, where $n = 60$ is the number of nodes and we do not deal with data at $j = 1$ since the PDE does not apply at $t = 0$. We can therefore convert (10) into a rectangular matrix problem $\mathbf{A}\theta = \mathbf{b}$, where the r th row in \mathbf{A} , $r = 1, \dots, n(M - 1)$, corresponding to the point (x_{ij}, t_j) is given by $\mathbf{a}_{ij} \in \mathbb{R}^{1 \times d}$, where

$$\mathbf{a}_{ij} = \left[\frac{d\varphi_1(q_{ij})}{dq} \left(\frac{\partial q_{ij}}{\partial x} \right)^2 + \varphi_1(q_{ij}) \frac{\partial^2 q_{ij}}{\partial x^2}, \quad \dots, \quad \frac{d\varphi_d(q_{ij})}{dq} \left(\frac{\partial q_{ij}}{\partial x} \right)^2 + \varphi_d(q_{ij}) \frac{\partial^2 q_{ij}}{\partial x^2} \right], \quad (11)$$

with each element of \mathbf{a}_{ij} corresponding to the contribution of the associated basis function in (10). Thus,

we obtain the system

$$\mathbf{A} = \begin{bmatrix} \mathbf{a}_{12} \\ \mathbf{a}_{22} \\ \vdots \\ \mathbf{a}_{nM} \end{bmatrix} \in \mathbb{R}^{n(M-1) \times d} \quad \text{and} \quad \mathbf{b} = \begin{bmatrix} \partial q_{12}/\partial t \\ \partial q_{22}/\partial t \\ \vdots \\ \partial q_{nM}/\partial t \end{bmatrix} \in \mathbb{R}^{n(M-1) \times 1}. \quad (12)$$

The solution of $\mathbf{A}\boldsymbol{\theta} = \mathbf{b}$, given by $\boldsymbol{\theta} = (\mathbf{A}^\top \mathbf{A})^{-1} \mathbf{A}^\top \mathbf{b}$, is obtained by minimising the residual $\|\mathbf{A}\boldsymbol{\theta} - \mathbf{b}\|_2^2$, which keeps all terms present in the learned model. We expect, however, just as in (8), that $\boldsymbol{\theta}$ is sparse so that $D(q)$ has very few terms, which makes the interpretation of these terms feasible [37, 38]. There are several ways that we could solve $\mathbf{A}\boldsymbol{\theta} = \mathbf{b}$ to obtain a sparse vector, such as with sparse regression [37], but in this work we take a *stepwise equation learning* approach inspired by stepwise regression [44] as this helps with both the exposition and modularity of our approach. For this approach, we first let $\mathcal{I} = \{1, \dots, d\}$ be the set of basis function indices. We let \mathcal{A}_k denote the set of *active coefficients* at the k th iteration, meaning the indices of non-zero values in $\boldsymbol{\theta}$, starting with $\mathcal{A}_1 = \mathcal{I}$. The set of indices of zero values in $\boldsymbol{\theta}$, $\mathcal{I}_k = \mathcal{I} \setminus \mathcal{A}_k$, is called the set of *inactive coefficients*. To obtain the next set, \mathcal{A}_{k+1} , from a current set \mathcal{A}_k , we apply the following steps:

1. Let the vector $\boldsymbol{\theta}_{\mathcal{A}}$ denote the solution to $\mathbf{A}\boldsymbol{\theta} = \mathbf{b}$ subject to the constraint that each inactive coefficient θ_i is zero, meaning $\theta_i = 0$ for $i \in \mathcal{I} \setminus \mathcal{A}$ for a given set of active coefficients \mathcal{A} . We compute $\boldsymbol{\theta}_{\mathcal{A}}$ by solving the reduced problem in which the inactive columns of \mathbf{A} are not included. The vector with $\mathcal{A} = \mathcal{A}_k$ at step k is denoted $\boldsymbol{\theta}_k$. With this definition, we compute the sets

$$\mathcal{M}_k^+ = \{\boldsymbol{\theta}_{\mathcal{A}_k \cup \{i\}} : i \notin \mathcal{A}_k\} \quad \text{and} \quad \mathcal{M}_k^- = \{\boldsymbol{\theta}_{\mathcal{A}_k \setminus \{i\}} : i \in \mathcal{A}_k\}. \quad (13)$$

\mathcal{M}_k^+ is the set of all coefficient vectors $\boldsymbol{\theta}$ obtained by making each active coefficient at step k inactive one at a time. \mathcal{M}_k^- , is similar to \mathcal{M}_{k+1}^- except we make each inactive coefficient at step k active one at a time. We then define $\mathcal{M}_k = \{\boldsymbol{\theta}_k\} \cup \mathcal{M}_k^+ \cup \mathcal{M}_k^-$, so that \mathcal{M}_k is the set of all coefficient vectors obtained from activating coefficients one at a time, deactivating coefficients one at a time, or retaining the current vector $\boldsymbol{\theta}_k$.

2. Choose one of the vectors in \mathcal{M}_k by defining a loss function $\mathcal{L}(\boldsymbol{\theta})$:

$$\underbrace{\mathcal{L}(\boldsymbol{\theta})}_{\text{loss}} = \underbrace{\log \left[\frac{1}{n(M-1)} \sum_{j=2}^M \sum_{i=1}^n \left(\frac{q_{ij} - q(x_{ij}, t_j; \boldsymbol{\theta})}{q_{ij}} \right)^2 \right]}_{\text{goodness of fit}} + \underbrace{\|\boldsymbol{\theta}\|_0}_{\text{model complexity}}, \quad (14)$$

where $q(x, t; \boldsymbol{\theta})$ is the solution of the PDE (7) with $R(q) = H(q) = 0$ and $D(q)$ uses the coefficients $\boldsymbol{\theta}$ in (9), $q(x_{ij}, t_j; \boldsymbol{\theta})$ is the linear interpolant of the PDE data at $t = t_j$ evaluated at $x = x_{ij}$, and $\|\boldsymbol{\theta}\|_0$ is the number of non-zero terms in $\boldsymbol{\theta}$. This loss function balances the goodness of fit with model complexity. If, for some $\boldsymbol{\theta}$, $D(q) < 0$ within $q_{\min} \leq q \leq q_{\max}$, which we check by evaluating $D(q)$ at $n_c = 100$ equally spaced points in $q_{\min} \leq q \leq q_{\max}$, we set $\mathcal{L}(\boldsymbol{\theta}) = \infty$. With this loss function, we compute the next coefficient vector

$$\boldsymbol{\theta}_{k+1} = \underset{\boldsymbol{\theta} \in \mathcal{M}_k}{\operatorname{argmin}} \mathcal{L}(\boldsymbol{\theta}). \quad (15)$$

If $\boldsymbol{\theta}_{k+1} = \mathbf{0}$, so that all the coefficients are inactive, we instead take the vector that attains the second-smallest loss so that a model with no terms cannot be selected.

3. If $\boldsymbol{\theta}_{k+1} = \boldsymbol{\theta}_k$, then there are no more local improvements to be made and so the procedure stops. Otherwise, we recompute \mathcal{A}_{k+1} and \mathcal{I}_{k+1} from $\boldsymbol{\theta}_{k+1}$ and continue iterating.

The second step prevents empty models from being returned, allowing the algorithm to more easily find an optimal model when starting with no active coefficients. We note that Nardini et al. [32] consider a loss based on the regression error, $\|\mathbf{A}\boldsymbol{\theta} - \mathbf{b}\|_2^2$, that has been useful for a range of previously-considered problems [32, 37, 38]. We do not consider the regression error in this work as we find that it typically leads to poorer estimates for $\boldsymbol{\theta}$ compared to controlling the density errors as we do in (15).

Let us now apply the procedure to our data from Figure 2, where we know that the continuum limit with $D(q) = 50/q^2$ is accurate. We use the basis functions $\varphi_i = 1/q^i$ for $i = 1, 2, 3$ so that

$$D(q) = \frac{\theta_1}{q} + \frac{\theta_2}{q^2} + \frac{\theta_3}{q^3}, \quad (16)$$

and we expect to learn $\boldsymbol{\theta} = (0, 50, 0)^\top$. We save the solution to the discrete model at $M = 50$ equally spaced time points between $t_1 = 0$ and $t_M = 5$. With this setup, and starting with all coefficients initially active so that $\mathcal{A}_1 = \{1, 2, 3\}$, we obtain the results in Table 2. The first iterate gives us $\boldsymbol{\theta}_1$ such that $D(q) < 0$ for some range of q as we show in Figure 4(a), and so we assign $\mathcal{L}(\boldsymbol{\theta}_1) = \infty$. To get to the next step, we remove θ_1 , θ_2 , and θ_3 one a time and compute the loss for each resulting vector, and we find that removing θ_3 leads to a vector that gives the least loss out of those considered. We thus find $\mathcal{A}_2 = \{1, 2\}$ and $\boldsymbol{\theta}_2 = (-1.46, 47.11, 0)^\top$. Continuing, we find that out of the choice of removing θ_1 or θ_2 , or putting θ_3 back into the model, removing θ_1 decreases the loss by the greatest amount, giving $\mathcal{A}_3 = \{2\}$. Finally, we find that there are no more improvements to be made, and so the algorithm stops at $\boldsymbol{\theta}_3 = (0, 43.52, 0)^\top$, which is close to the continuum limit. We emphasise that this final $\boldsymbol{\theta}_3$ is a least squares solution with the constraint $\theta_1 = \theta_3 = 0$, thus there is no need to refine $\boldsymbol{\theta}_3$ further by eliminating θ_1 and θ_3 directly in (16), as the result would be the same. Comparing the densities from the solution of the learned PDE with $\boldsymbol{\theta} = \boldsymbol{\theta}_3$ with the discrete densities in Figure 5(a), we see that the curves are nearly visually indistinguishable near the center, but there are some visually discernible discrepancies near the boundaries. We show the form of $D(q)$ at each iteration in Figure 4(a), where we observe that the first iterate captures only the higher densities, the second iterate captures the complete range of densities, and the third iterate removes a single term which gives no noticeable difference.

Table 2: Stepwise equation learning results for the density data for Case Study 1: Fixed boundaries using the basis expansion (16), saving the results at $M = 50$ equally spaced times between $t_1 = 0$ and $t_M = 5$ and starting with all coefficients active, $\mathcal{A}_1 = \{1, 2, 3\}$. Coefficients highlighted in blue show the coefficient chosen to be removed or added at the corresponding step.

Step	θ_1	θ_2	θ_3	Loss
1	-5.97	70.73	-27.06	∞
2	-1.46	47.11	0.00	-4.33
3	0.00	43.52	0.00	-5.18

To improve our learned model we introduce *matrix pruning*, inspired from the data thresholding approach in VandenHeuvel et al. [42], to improve the estimates for $\boldsymbol{\theta}$. Visual inspection of the space-time diagram in Figure 2(a) shows that the most significant density changes occur at early time and near to locations where q changes in the initial condition, and a significant portion of the space-time diagram involves regions where q is almost constant. These regions where q has minimal change are problematic as points which lead to a higher residual are overshadowed, affecting the least squares problem and consequently degrading the estimates for $\boldsymbol{\theta}$ significantly, and so it is useful to only include important points in the construction of \mathbf{A} . To resolve this issue, we choose to only include points if the associated densities falls between the 10% and 90% quantiles for the complete set of densities, which we refer to by *density quantiles*; more details on this pruning procedure are given in Appendix D. This choice of density quantiles is made using trial and error, starting at 0% and 100%, respectively, and shrinking the quantile range until suitable results are obtained. When we apply this pruning and reconstruct \mathbf{A} , we obtain the improved results in Table 3 and associated densities in Figure 5(b). Compared with Table 2, we see that the coefficient estimates for $\boldsymbol{\theta}$ all lead to improved losses, and our final model now has $\boldsymbol{\theta} = (0, 49.83, 0)^\top$, which is much closer to the continuum limit, as we see in Figure 5(b) where the solution curves are now visually indistinguishable

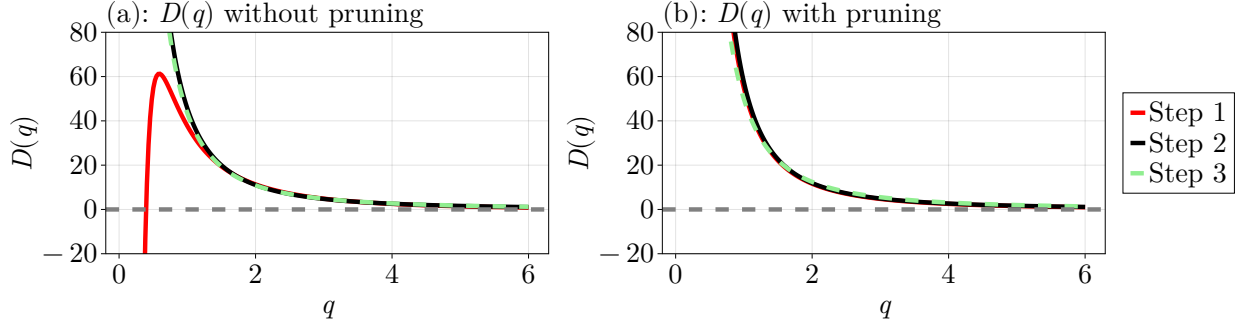


Figure 4: Progression of $D(q)$ over each iterate for Case Study 1: Fixed boundaries. (a) Progression from the results in Table 2 (dashed curves). (b) As in (a), except with the results from Table 3 using matrix pruning.

everywhere. Moreover, we show in Figure 4(b) how $D(q)$ is updated at each iteration, where we see that the learned nonlinear diffusivity functions are barely different from the expected continuum limit result. These results demonstrate the importance of only including the most important points in \mathbf{A} .

Table 3: Improved results for Case Study 1: Fixed boundaries from Table 2, now using matrix pruning so that densities outside of the 10% and 90% density quantiles are not included. Coefficients highlighted in blue show the coefficient chosen to be removed or added at the corresponding step.

Step	θ_1	θ_2	θ_3	Loss
1	-1.45	42.48	13.76	-4.19
2	0.00	37.79	19.69	-5.46
3	0.00	49.83	0.00	-7.97

4.2 Case Study 2: Free boundaries

Case Study 2 extends Case Study 1 by allowing the right-most cell boundary to move so that $H(q) \neq 0$. We do not consider proliferation, giving $R(q) = 0$ in (7).

The equation learning procedure for this case study is similar to Case Study 1, namely we expand $D(q)$ as in (9) and constrain $D(q) \geq 0$. In addition to learning $D(q)$, we need to learn $H(q)$ and the evolution equation describing the free boundary. In (7), this evolution equation is given by a conservation statement, $q dL/dt = -D(q) \partial q / \partial x$ with $q = q(L(t), t)$. Here we treat this moving boundary condition more generally by introducing a function $E(t)$ so that

$$q \frac{dL}{dt} = -E(q) \frac{\partial q}{\partial x} \quad (17)$$

at $x = L(t)$ for $t > 0$. While (17) could lead to local loss of conservation at the moving boundary, our approach is to for the possibility that coefficients in $D(q)$ and $E(q)$ differ and to explore the extent to which this is true, or otherwise, according to our equation learning procedure. We constrain $E(q) \geq 0$ so that (17) makes sense for our problem and we expand $D(q)$, $H(q)$, and $E(q)$ as follows

$$D(q) = \sum_{i=1}^d \theta_i^d \varphi_i^d(q), \quad H(q) = \sum_{i=1}^h \theta_i^h \varphi_i^h(q), \quad E(q) = \sum_{i=1}^h \theta_i^e \varphi_i^e(q). \quad (18)$$

The matrix system for $\boldsymbol{\theta}^d = (\theta_1^d, \dots, \theta_d^d)^\top$ is the same as it was in Case Study 1 in (12), which we now write as $\mathbf{A}^d \boldsymbol{\theta}^d = \mathbf{b}^d$ with $\mathbf{A}^d \in \mathbb{R}^{n(M-1) \times d}$ and $\mathbf{b}^d \in \mathbb{R}^{n(M-1) \times 1}$ given by \mathbf{A} and \mathbf{b} in (12), and we can construct two other independent matrix systems for $\boldsymbol{\theta}^h = (\theta_1^h, \dots, \theta_h^h)^\top$ and $\boldsymbol{\theta}^e = (\theta_1^e, \dots, \theta_e^e)^\top$. To construct these

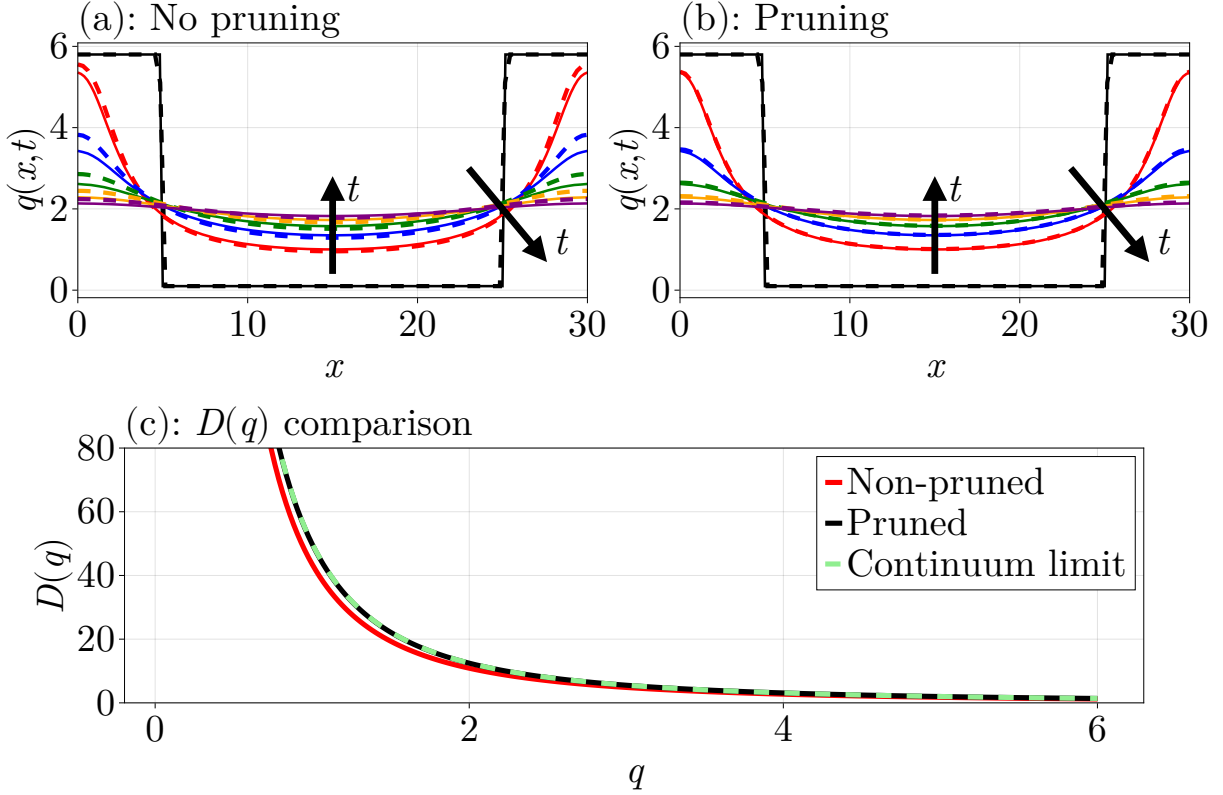


Figure 5: Stepwise equation learning results for Case Study 1: Fixed boundaries. (a) Comparisons of the discrete density profiles (solid curves) with those learned from PDEs obtained from the results in Table 2 (dashed curves). (b) As in (a), except with the results from Table 3 using matrix pruning so that densities outside of the 10% and 90% density quantiles are not included. (c) Comparisons of the learned $D(q)$ from Table 2 without pruning, Table 3 with pruning, and the continuum limit from (8). In (a)–(b), the arrows show the direction of increasing time, and the density profiles shown are at times $t = 0, 1, 2, 3, 4, 5$ in black, red, blue, green, orange, and purple, respectively.

matrix systems, for a given boundary point (x_{nj}, t_j) we write

$$\frac{\partial q_{nj}}{\partial x} = \sum_{k=1}^h \theta_k^h \varphi_k^h(q_{nj}), \quad q_{nj} \frac{dL_j}{dt} = -\frac{\partial q_{nj}}{\partial x} \sum_{k=1}^e \theta_k^e \varphi_k^e(q_{nj}), \quad (19)$$

where $L_j = x_{nj}$ is the position of the leading edge at $t = t_j$. In (19) we assume that L_j can be approximated by a smooth function so that dL_j/dt can be defined. With (19) we have $\mathbf{A}^h \boldsymbol{\theta}^h = \mathbf{b}^h$ and $\mathbf{A}^e \boldsymbol{\theta}^e = \mathbf{b}^e$, where

$$\mathbf{A}^h = \begin{bmatrix} \varphi_1^h(q_{12}) & \cdots & \varphi_h^h(q_{12}) \\ \vdots & \ddots & \vdots \\ \varphi_1^h(q_{nM}) & \cdots & \varphi_h^h(q_{nM}) \end{bmatrix}, \quad \mathbf{b}^h = \begin{bmatrix} \frac{\partial q_{12}}{\partial x} \\ \vdots \\ \frac{\partial q_{nM}}{\partial x} \end{bmatrix} \quad (20)$$

with $\mathbf{A}^h \in \mathbb{R}^{(M-1) \times h}$ and $\mathbf{b}^h \in \mathbb{R}^{(M-1) \times 1}$, and

$$\mathbf{A}^e = \begin{bmatrix} \varphi_1^e(q_{12}) \frac{\partial q_{n2}}{\partial x} & \cdots & \varphi_e^e(q_{12}) \frac{\partial q_{n2}}{\partial x} \\ \vdots & \ddots & \vdots \\ \varphi_1^e(q_{nM}) \frac{\partial q_{nM}}{\partial x} & \cdots & \varphi_e^e(q_{nM}) \frac{\partial q_{nM}}{\partial x} \end{bmatrix}, \quad \mathbf{b}^e = - \begin{bmatrix} q_{n2} \frac{dL_2}{dt} \\ \vdots \\ q_{nM} \frac{dL_M}{dt} \end{bmatrix} \quad (21)$$

with $\mathbf{A}^e \in \mathbb{R}^{(M-1) \times e}$ and $\mathbf{b}^e \in \mathbb{R}^{(M-1) \times 1}$. Then, writing

$$\mathbf{A} = \text{diag}(\mathbf{A}^d, \mathbf{A}^h, \mathbf{A}^e) \in \mathbb{R}^{(n+2)(M-1) \times (d+h+e)}, \quad \mathbf{b} = \begin{bmatrix} \mathbf{b}^d \\ \mathbf{b}^h \\ \mathbf{b}^e \end{bmatrix} \in \mathbb{R}^{(n+2)(M-1) \times 1}, \quad (22)$$

we obtain

$$\mathbf{A}\boldsymbol{\theta} = \mathbf{b}, \quad \boldsymbol{\theta} = \begin{bmatrix} \boldsymbol{\theta}^d \\ \boldsymbol{\theta}^h \\ \boldsymbol{\theta}^e \end{bmatrix} \in \mathbb{R}^{(d+h+e) \times 1}. \quad (23)$$

The solution of $\mathbf{A}\boldsymbol{\theta} = \mathbf{b}$ is the combined solution of the individual linear systems as \mathbf{A} is block diagonal. Estimates for $\boldsymbol{\theta}^d$, $\boldsymbol{\theta}^h$, and $\boldsymbol{\theta}^e$ are independent, which demonstrates the modularity of our approach, where these additional features, in particular the leading edge, are just an extra independent component of our procedure in addition to the procedure for estimating $D(q)$.

In addition to the new matrix system $\mathbf{A}\boldsymbol{\theta} = \mathbf{b}$ in (23), we augment the loss function (14) to incorporate information about the location of the moving boundary. Letting $L(t; \boldsymbol{\theta})$ denote the leading edge from the solution of the PDE (7) with parameters $\boldsymbol{\theta}$, the loss function is

$$\underbrace{\mathcal{L}(\boldsymbol{\theta})}_{\text{loss}} = \underbrace{\log \left[\frac{1}{n(M-1)} \sum_{j=2}^M \sum_{i=1}^n \left(\frac{q_{ij} - q(x_{ij}, t_j; \boldsymbol{\theta})}{q_{ij}} \right)^2 \right]}_{\text{density goodness of fit}} + \underbrace{\log \left[\frac{1}{M-1} \sum_{j=2}^M \left(\frac{L_j - L(t_j; \boldsymbol{\theta})}{L_j} \right)^2 \right]}_{\text{leading edge goodness of fit}} + \underbrace{\|\boldsymbol{\theta}\|_0}_{\text{model complexity}}. \quad (24)$$

Let us now apply our stepwise equation learning procedure with (23) and (24). We consider the data from Figure 2, where we know in advance that the continuum limit with $D(q) = 50/q^2$, $H(q) = 2q^2 - 0.4q^3$, and $E(q) = 50/q^2$ is accurate. The expansions we use for $D(q)$, $H(q)$, and $E(q)$ are given by

$$\begin{aligned} D(q) &= \frac{\theta_1^d}{q} + \frac{\theta_2^d}{q^2} + \frac{\theta_3^d}{q^3}, \\ H(q) &= \theta_1^h q + \theta_2^h q^2 + \theta_3^h q^3 + \theta_4^h q^4 + \theta_5^h q^5, \\ E(q) &= \frac{\theta_1^e}{q} + \frac{\theta_2^e}{q^2} + \frac{\theta_3^e}{q^3}. \end{aligned} \quad (25)$$

With these expansions, we expect to learn $\boldsymbol{\theta}^d = (0, 50, 0)^\top$, $\boldsymbol{\theta}^h = (0, 2, -0.4, 0, 0)^\top$, and $\boldsymbol{\theta}^e = (0, 50, 0)^\top$. We initially consider saving the solution at $M = 1000$ equally spaced times between $t_1 = 0$ and $t_M = 100$, and using matrix pruning so that only points whose densities fall within the 35% and 65% density quantiles are included. The results with this configuration are shown in Table 4, where we see that we are only able to learn $H(q) = E(q) = 0$ and $D(q) = 25.06/q^3$. This outcome highlights the importance of choosing an appropriate time interval, since Figure 2(b) indicates that mechanical relaxation takes place over a relative short interval which means that working with data in $0 < t \leq 100$ can lead to a poor outcome.

Table 4: Stepwise equation learning results for Case Study 2: Free boundaries, using the basis expansions (25), saving the results at $M = 1000$ equally spaced times between $t_1 = 0$ and $t_M = 100$, pruning so that densities outside of the 35% and 65% density quantiles are not included, and starting with all terms inactive. Coefficients highlighted in blue show the coefficient chosen to be removed or added at the corresponding step.

Step	θ_1^d	θ_2^d	θ_3^d	θ_1^h	θ_2^h	θ_3^h	θ_4^h	θ_5^h	θ_1^e	θ_2^e	θ_3^e	Loss
1	0.00	0.00	0.00	0.00	0.00	0.00	0.00	0.00	0.00	0.00	0.00	-1.40
2	0.00	0.00	25.06	0.00	0.00	0.00	0.00	0.00	0.00	0.00	0.00	-0.40

We proceed by restricting our data collection to $0 \leq t \leq 15$, now saving the solution at $M = 200$ equally spaced times between $t_1 = 0$ and $t_M = 15$. Keeping the same quantiles for the matrix pruning, the new results are shown in Table 5 and Figure 6. We see that the densities and leading edges are accurate for small time, but the learned mechanisms do not extrapolate as well for $t \geq 15$, for example $L(t)$ in Figure 6(b) does not match the discrete data. To address this issue, we can further limit the information that we include in our matrices, looking to only include boundary points where dL/dt is neither too large nor too small. We implement this by excluding all points (x_{n_j}, t_j) from the construction of $(\mathbf{A}^e, \mathbf{b}^e)$ in (21) such that dL_j/dt is outside of the 10% or 90% quantiles of the vector $(dL_2/dt, \dots, dL_M/dt)$, called the *velocity quantiles*.

Table 5: Stepwise equation learning results for Case Study 2: Free boundaries, using the basis expansions (25), saving the results at $M = 200$ equally spaced times between $t_1 = 0$ and $t_M = 15$, pruning so that densities outside of the 35% and 65% density quantiles are not included, and starting with all terms inactive. Coefficients highlighted in blue show the coefficient chosen to be removed or added at the corresponding step.

Step	θ_1^d	θ_2^d	θ_3^d	θ_1^h	θ_2^h	θ_3^h	θ_4^h	θ_5^h	θ_1^e	θ_2^e	θ_3^e	Loss
1	0.00	0.00	0.00	0.00	0.00	0.00	0.00	0.00	0.00	0.00	0.00	-3.37
2	0.00	0.00	0.00	0.00	-0.03	0.00	0.00	0.00	0.00	0.00	0.00	-2.37
3	0.00	0.00	0.00	0.00	-0.03	0.00	0.00	0.00	8.74	0.00	0.00	-3.68
4	0.00	47.38	0.00	0.00	-0.03	0.00	0.00	0.00	8.74	0.00	0.00	-4.02
5	0.00	47.38	0.00	8.41	-1.69	0.00	0.00	0.00	8.74	0.00	0.00	-8.14

Implementing thresholding on dL/dt leads to the results presented in Figure 7. We see that the learned densities and leading edges are both visually indistinguishable from the discrete data. Since $H(q)$ and $E(q)$ are only ever evaluated at $x = L(t)$, and $q(L(t), t) \approx 5$ for $t > 0$, we see that $H(q)$ and $E(q)$ only match the continuum limit at $q \approx 5$, which means that our learned continuum limit model conserves mass and is consistent with the traditional coarse-grained continuum limit, as expected. We discuss in Appendix E how we can enforce $D(q) = E(q)$ to guarantee conservation mass from the outset, however our approach in Figure 7 is more general in the sense that our learned continuum limit is obtained without making any *a priori* assumptions about the form of $E(q)$.

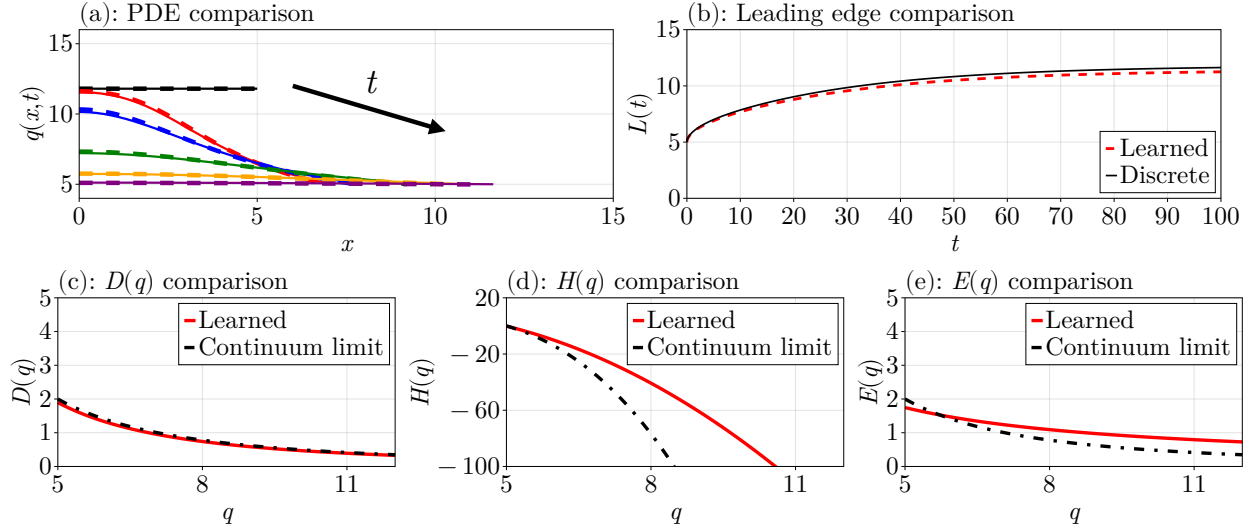


Figure 6: Stepwise equation learning results from Table 5 for Case Study 2: Free boundaries. (a) Comparisons of the discrete density profiles (solid curves) with those learned from PDEs obtained from the results in Table 5 (dashed curves), plotted at the times $t = 0, 5, 10, 25, 50, 100$ in black, red, blue, green, orange, and purple, respectively. The arrow shows the direction of increasing time. (b) As in (a), except comparing the leading edges. (c)–(e) are comparisons of the learned forms of $D(q)$, $H(q)$, and $E(q)$ with the forms from the continuum limit (8).

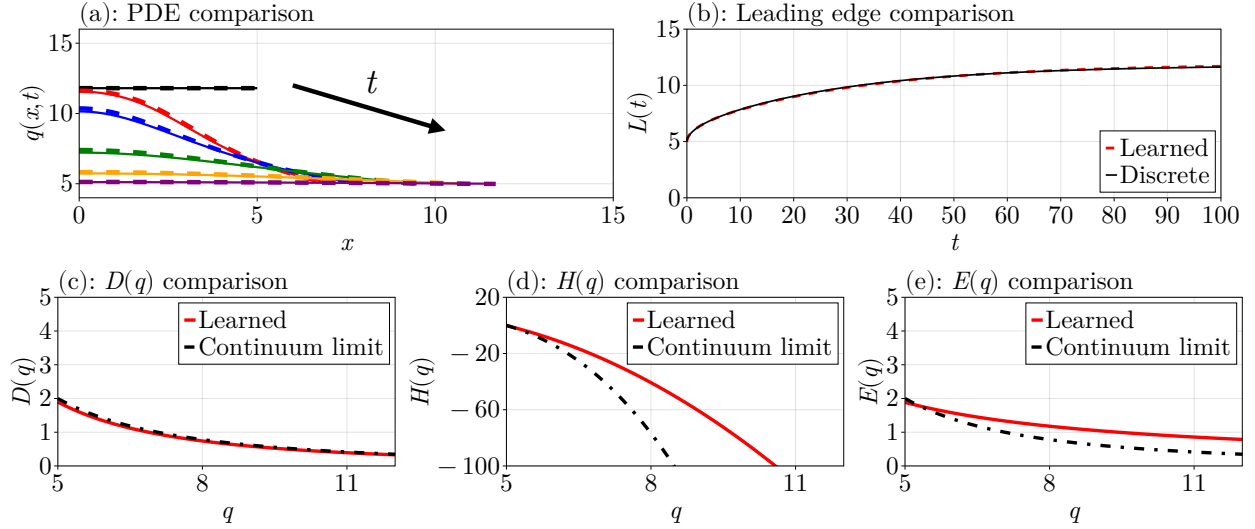


Figure 7: Stepwise equation learning results from Table 5 for Case Study 2: Free boundaries, except also using matrix pruning on $(\mathbf{A}_3, \mathbf{b}_3)$ so points where dL_j/dt falls outside of the 10% and 90% velocity quantiles are excluded, giving $\theta_1^e = 9.42$ rather than 8.74. (a) Comparisons of the discrete density profiles (solid curves) with those from the learned PDE (dashed curves), plotted at the times $t = 0, 5, 10, 25, 50, 100$ in black, red, blue, green, orange, and purple, respectively. The arrow shows the direction of increasing time. (b) As in (a), except comparing the leading edges. (c)–(e) are comparisons of the learned forms of $D(q)$, $H(q)$, and $E(q)$ with the forms from the continuum limit (8).

4.3 Case Study 3: Fixed boundaries with proliferation

Case Study 3 is identical to Case Study 1 except that we incorporate cell proliferation, implying $R(q) \neq 0$ in (7). This case is more complicated than with mechanical relaxation only, as we have to consider how we combine the repeated realisations to capture the average density data as well. For this work, we average over each realisation at each time using linear interpolants as described in Appendix D. This averaging procedure gives n_k points \bar{x}_{ij} between $x = 0$ and $x = 30$ at each time t_j , $j = 1, \dots, M$, with corresponding density value \bar{q}_{ij} . The quantities \bar{x}_{ij} and \bar{q}_{ij} play the same role as x_{ij} and q_{ij} in the previous case studies.

To apply equation learning we note there is no moving boundary, giving $H(q) = 0$ in (8). We proceed by expanding $D(q)$ and $R(q)$ as follows

$$D(q) = \sum_{i=1}^d \theta_i^d \varphi_i^d(q), \quad R(q) = \sum_{i=1}^r \theta_i^r \varphi_i^r(q), \quad (26)$$

with the aim of estimating $\boldsymbol{\theta}^d = (\theta_1^d, \dots, \theta_d^d)^\top$ and $\boldsymbol{\theta}^r = (\theta_1^r, \dots, \theta_r^r)^\top$, again constraining $D(q) \geq 0$. We expand the PDE from (10), as in Section 4(a), and the only difference is the additional term $\sum_{m=1}^r \varphi_m^r(\bar{q}_{ij}) \theta_m^r$ for each point (\bar{x}_{ij}, t_j) . Thus, we have the same matrix as in Section 4(a), denoted $\mathbf{A}^d \in \mathbb{R}^{n_k(M-1) \times d}$, and a new matrix $\mathbf{A}^r \in \mathbb{R}^{n_k(M-1) \times r}$ whose row corresponding to the point (\bar{x}_{ij}, t_j) is given by

$$\mathbf{a}_{ij}^r = [\varphi_1^r(\bar{q}_{ij}) \quad \dots \quad \varphi_r^r(\bar{q}_{ij})] \in \mathbb{R}^{1 \times r}, \quad (27)$$

so that the coefficient matrix \mathbf{A} is now

$$\mathbf{A} = [\mathbf{A}^d \quad \mathbf{A}^r] \in \mathbb{R}^{n_k(M-1) \times (d+r)}. \quad (28)$$

The corresponding entry for the point (\bar{x}_{ij}, t_j) in $\mathbf{b} \in \mathbb{R}^{n_k(M-1) \times 1}$ is $\partial \bar{q}_{ij} / \partial t$. Notice that this additional term in the PDE adds an extra block to the matrix without requiring a significant coupling with the existing equations from the simpler problem without proliferation. Thus, we estimate our coefficient vectors using the system

$$\mathbf{A}\boldsymbol{\theta} = \mathbf{b}, \quad \boldsymbol{\theta} = \begin{bmatrix} \boldsymbol{\theta}^d \\ \boldsymbol{\theta}^r \end{bmatrix} \in \mathbb{R}^{(d+r) \times 1}. \quad (29)$$

We can take exactly the same stepwise procedure as in Section 4(a), except now the loss function (14) uses n_k , \bar{q}_{ij} , and \bar{x}_{ij} rather than n , q_{ij} , and x_{ij} , respectively.

4.3.1 Accurate continuum limit

Let us now apply these ideas to our data from Figure 2, where we know that the continuum limit with $D(q) = 50/q^2$ and $R(q) = 0.15q - 0.01q^2$ is accurate. The expansions we use for $D(q)$ and $R(q)$ are given by

$$D(q) = \frac{\theta_1^d}{q} + \frac{\theta_2^d}{q^2} + \frac{\theta_3^d}{q^3}, \quad R(q) = \theta_1^r q + \theta_2^r q^2 + \theta_3^r q^3 + \theta_4^r q^4 + \theta_5^r q^5, \quad (30)$$

and we expect to learn $\boldsymbol{\theta}^d = (0, 50, 0)^\top$ and $\boldsymbol{\theta}^r = (0.15, -0.01, 0, 0, 0)^\top$. We average over 1000 identically-prepared realisations, saving the solutions at $M = 501$ equally spaced times between $t_1 = 0$ and $t_M = 50$ with $n_k = 50$ knots for averaging. For this problem, and for Case Study 4 discussed later, we find that working with 1000 identically-prepared realisations of the stochastic models leads to sufficiently smooth density profiles. As discussed in Appendix F, the precise number of identically-prepared realisations is not important provided that the number is sufficiently large; when not enough realisations are taken, the results are inconsistent across different sets of realisations and will fail to identify the average behaviour from the learned model. We also use matrix pruning so that we only include points whose densities fall within the 10% and 90% density quantiles, as done in Section 4(a). The results we obtain are shown in Table 6, starting with all coefficients active.

Table 6 shows that we find $\boldsymbol{\theta}^d = (0, 52.97, 0)^\top$ and $\boldsymbol{\theta}^r = (0.15, -0.010, 0, 0, 0)^\top$, which are both very close to the continuum limit. Figure 8 visualises these results, showing that the PDE solutions with the learned $D(q)$ and $R(q)$ match the discrete densities, and the mechanisms that we do learn are visually indistinguishable with the continuum limit functions (8) as shown in Figure 8(b)–(c).

Table 6: Stepwise equation learning results for Case Study 3: Fixed boundaries with proliferation, where the continuum limit is accurate, using the basis expansions (30), saving the results at $M = 501$ equally spaced times between $t_1 = 0$ and $t_M = 50$, averaging across 1000 realisations with $n_k = 50$ knots, pruning so that densities outside of the 10% and 90% density quantiles are not included, and starting with all diffusion and reaction coefficients active. Coefficients highlighted in blue show the coefficient chosen to be removed or added at the corresponding step.

Step	θ_1^d	θ_2^d	θ_3^d	θ_1^r	θ_2^r	$\theta_3^r (\times 10^{-4})$	$\theta_4^r (\times 10^{-5})$	$\theta_5^r (\times 10^{-7})$	Loss
1	-11.66	147.43	-191.51	0.13	-0.00	-0.00	5.83	-11.30	∞
2	-2.24	60.86	0.00	0.13	-0.00	-5.72	2.62	-3.49	-0.71
3	-2.25	60.90	0.00	0.14	-0.01	0.00	-1.25	5.95	-1.92
4	0.00	52.95	0.00	0.14	-0.01	0.00	-1.36	6.49	-3.35
5	0.00	53.02	0.00	0.15	-0.01	0.00	0.00	0.32	-4.98
6	0.00	52.97	0.00	0.15	-0.01	0.00	0.00	0.00	-5.70

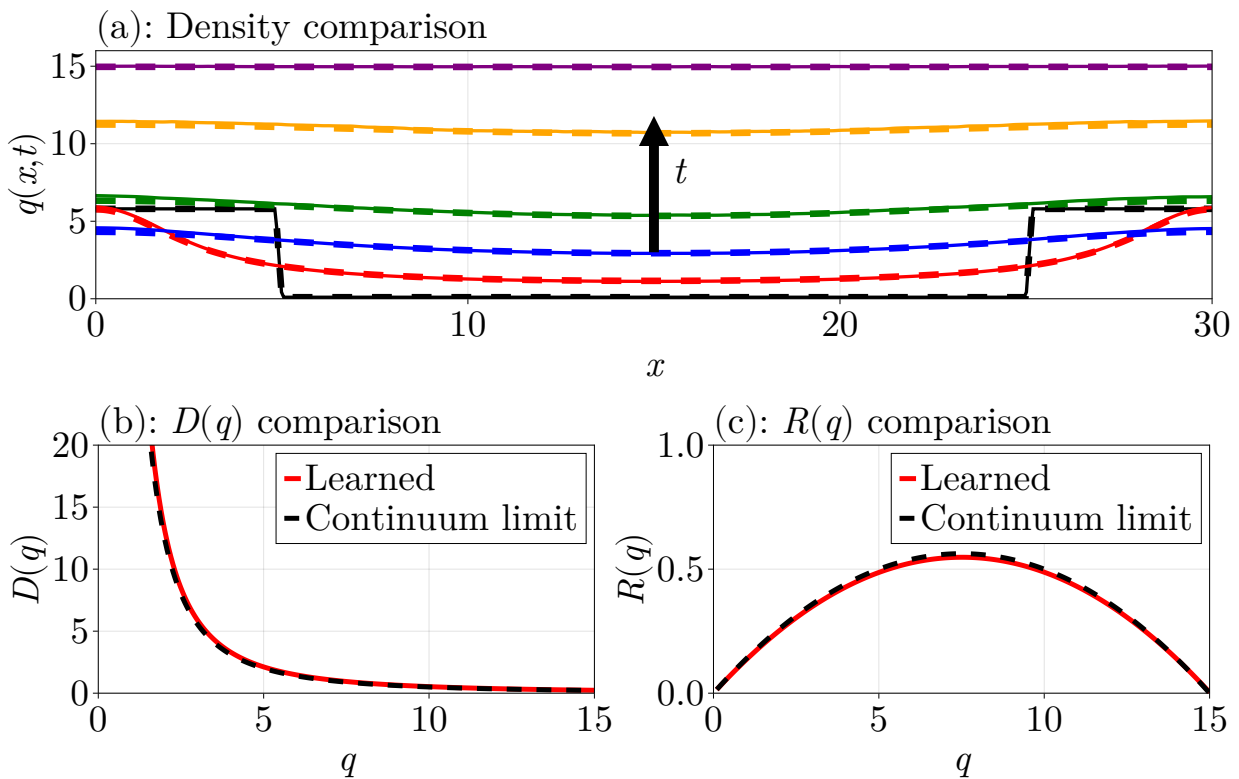


Figure 8: Stepwise equation learning results for Case Study 3: Fixed boundaries with proliferation, where the continuum limit is accurate. (a) Comparisons of the discrete density profiles (solid curves) with those learned from PDEs obtained from the results in Table 6 (dashed curves), plotted at the times $t = 0, 1, 5, 10, 20, 50$ in black, red, blue, green, orange, and purple, respectively. The arrow shows the direction of increasing time. (b)–(c) are comparisons of $D(q)$ and $R(q)$ with the forms from the continuum limit (8).

4.3.2 Inaccurate continuum limit

We now extend the problem so that the continuum limit is no longer accurate, taking $k = 1/5$ to be consistent with Figure 3(a). Using the same basis expansions in (30), we save the solution at $M = 751$ equally spaced

times between $t_1 = 0$ and $t_M = 75$, averaging over 1000 realisations with $n_k = 200$. We find that we need to use the 25% and 75% density quantiles rather than the 10% and 90% density quantiles, as in the previous example, to obtain results in this case. With this configuration, the results we find are shown in Table 7 and Figure 9.

Table 7: Stepwise equation learning results for Case Study 3: Fixed boundaries with proliferation, where the continuum limit is inaccurate, using the basis expansions (30), saving the results at $M = 751$ equally spaced times between $t_1 = 0$ and $t_M = 75$, averaging across 1000 realisations with $n_k = 200$ knots, pruning so that densities outside of the 25% and 75% density quantiles are not included, and starting with all diffusion and reaction coefficients inactive. Coefficients highlighted in blue show the coefficient chosen to be removed or added at the corresponding step.

Step	θ_1^d	θ_2^d	θ_3^d	θ_1^r	θ_2^r	$\theta_3^r (\times 10^{-4})$	$\theta_4^r (\times 10^{-5})$	θ_5^r	Loss
1	0.00	0.00	0.00	0.00	0.00	0.00	0.00	0.00	-0.33
2	0.00	0.00	0.00	0.02	0.00	0.00	0.00	0.00	0.51
3	0.00	0.00	0.00	0.11	-0.01	0.00	0.00	0.00	0.20
4	0.00	0.11	0.00	0.11	-0.01	0.00	0.00	0.00	-0.04
5	0.00	0.12	0.00	0.13	-0.01	1.59	0.00	0.00	-0.46
6	0.00	0.12	0.00	0.16	-0.02	7.49	-1.69	0.00	-1.13

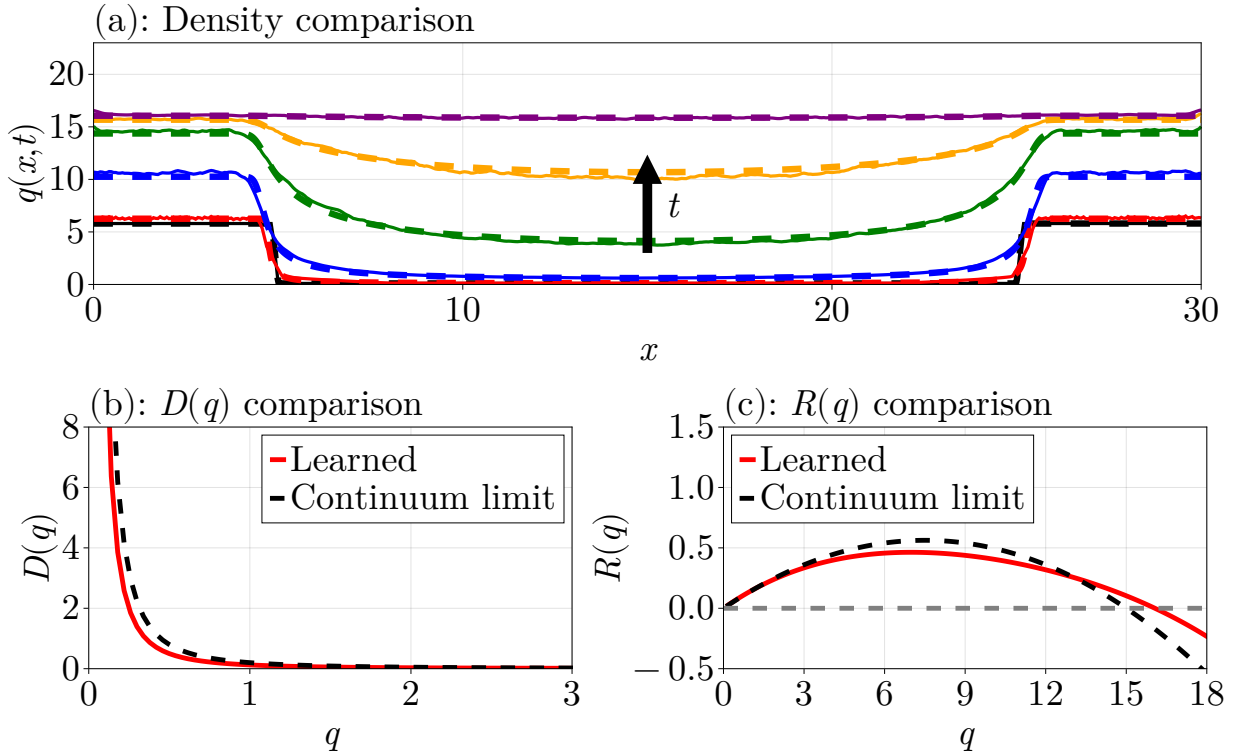


Figure 9: Stepwise equation learning results for Case Study 3: Fixed boundaries with proliferation, where the continuum limit is inaccurate. (a) Comparisons of the discrete density profiles (solid curves) with those learned from PDEs obtained from the results in Table 6 (dashed curves), plotted at the times $t = 0, 1, 10, 25, 40, 75$ in black, red, blue, green, orange, and purple, respectively. The arrow shows the direction of increasing time. (b)–(c) are comparisons of $D(q)$ and $R(q)$ with the forms from the continuum limit (8).

Results in Table 7 show $\boldsymbol{\theta}^d = (0, 0.12, 0)^\top$, which is reasonably close to the continuum limit with $(0, 0.2, 0)^\top$. The reaction vector, for which the continuum limit is $(0.15, -0.01, 0, 0, 0)^\top$ so that $R(q)$ is a quadratic, is now given by $\boldsymbol{\theta}^r = (0.16, -0.02, 7.49 \times 10^{-4}, -1.69 \times 10^{-5}, 0)^\top$, meaning the learned $R(q)$ is a quartic. Figure 9 compares the averaged discrete densities with the solution of the learned continuum limit model. Figure 9(c) compares the learned source term with the continuum limit. While both terms are visually indistinguishable at small densities, we see that the two source terms differ at high densities, with the learned carrying capacity density, where $R(q) = 0$, reduced relative to the continuum limit. This is consistent with previous results [15].

4.4 Case Study 4: Free boundaries with proliferation

Case Study 4 is identical to Case Study 2 except that we now introduce proliferation into the discrete model so that $R(q) \neq 0$ in (7). First, as in Case Study 3 and as described in Appendix D, we average our data across each realisation from our discrete model. This averaging provides us with points \bar{x}_{ij} between $x = 0$ and $x = \bar{L}_j$ at each time t_j , $j = 1, \dots, M$, where \bar{L}_j is the average leading edge at $t = t_j$, with corresponding density values \bar{q}_{ij} , where $i = 1, \dots, n_k$ and n_k is the number of knots to use for averaging. We expand the functions $D(q)$, $R(q)$, $H(q)$, and $E(q)$ as

$$D(q) = \sum_{i=1}^d \theta_i^d \varphi_i^d(q), \quad R(q) = \sum_{i=1}^r \theta_i^r \varphi_i^r(q), \quad H(q) = \sum_{i=1}^h \theta_i^h \varphi_i^h(q), \quad E(q) = \sum_{i=1}^e \theta_i^e \varphi_i^e(q), \quad (31)$$

again restricting $D(q), E(q) \geq 0$. The function $E(q)$ is used in the moving boundary condition in (7), as in (17). The matrix \mathbf{A} and vector \mathbf{b} are given by

$$\mathbf{A} = \text{diag}(\mathbf{A}^{dr}, \mathbf{A}^h, \mathbf{A}^e) \in \mathbb{R}^{n_k(M-1) \times (d+r+h+e)}, \quad \mathbf{b} = \begin{bmatrix} \mathbf{b}^{dr} \\ \mathbf{b}^h \\ \mathbf{b}^e \end{bmatrix} \in \mathbb{R}^{n_k(M-1)}, \quad (32)$$

where $\mathbf{A}^{dr} = [\mathbf{A}^d \mathbf{A}^r]$ as defined in (28), \mathbf{A}^h and \mathbf{A}^e are the matrices from (20) and (21), respectively, and similarly for $\mathbf{b}^{dr} = \partial \mathbf{q} / \partial t$, \mathbf{b}^h , and \mathbf{b}^e from (12), (20), and (21), respectively. Thus,

$$\mathbf{A}\boldsymbol{\theta} = \mathbf{b}, \quad \boldsymbol{\theta} = \begin{bmatrix} \boldsymbol{\theta}^d \\ \boldsymbol{\theta}^r \\ \boldsymbol{\theta}^h \\ \boldsymbol{\theta}^e \end{bmatrix} \in \mathbb{R}^{(d+r+h+e) \times 1}. \quad (33)$$

Similar to Case Study 2, the coefficients for each mechanism are independent, except for $\boldsymbol{\theta}^d$ and $\boldsymbol{\theta}^r$. The loss function we use is the loss function from (24).

With this problem, it is difficult to learn all mechanisms simultaneously, especially as mechanical relaxation and proliferation occur on different time scales since mechanical relaxation dominates in the early part of the simulation, whereas both proliferation and mechanical relaxation play a role at later times. This means $D(q)$ and $R(q)$ cannot be estimated over the entire time range as was done in Case Study 3. To address this we take a sequential learning procedure to learn these four mechanisms using four distinct time intervals I^d , I^e , I^h , and I^r :

1. Fix $R(q) = H(q) = E(q) = 0$ and learn $\boldsymbol{\theta}^d$ over $t \in I^d$, solving $\mathbf{A}^d \boldsymbol{\theta}^d = \mathbf{b}^{dr}$.
2. Fix $R(q) = H(q) = 0$ and $\boldsymbol{\theta}^d$ and learn $\boldsymbol{\theta}^e$ over $t \in I^e$, solving $\mathbf{A}^e \boldsymbol{\theta}^e = \mathbf{b}^e$.
3. Fix $R(q) = 0$, $\boldsymbol{\theta}^d$, and $\boldsymbol{\theta}^e$ and learn $\boldsymbol{\theta}^h$ over $t \in I^h$, solving $\mathbf{A}^h \boldsymbol{\theta}^h = \mathbf{b}^h$.
4. Fix $\boldsymbol{\theta}^d$, $\boldsymbol{\theta}^e$, and $\boldsymbol{\theta}^h$ and learn $\boldsymbol{\theta}^r$ over $t \in I^r$, solving $\mathbf{A}^r \boldsymbol{\theta}^r = \mathbf{b}^{dr} - \mathbf{A}^d \boldsymbol{\theta}^d$.

In these steps, solving the system $\mathbf{A}\boldsymbol{\theta} = \mathbf{b}$ means to apply our stepwise procedure to this system; for these problems, we start each procedure with no active coefficients. The modularity of our approach makes this sequential learning approach straightforward to implement. For these steps, the interval I^d must be over sufficiently small times so that proliferation does not dominate, noting that fixing $R(q) = 0$ will not allow us to identify any proliferation effects when estimating the parameters. This is less relevant for I^h and I^e as the estimates of $\boldsymbol{\theta}^h$ and $\boldsymbol{\theta}^e$ impact the moving boundary only.

4.5 Accurate continuum limit

We apply this procedure to data from Figure 2, where the continuum limit is accurate with $D(q) = 50/q^2$, $R(q) = 0.15q - 0.01q^2$, $H(q) = 2q^2 - 0.4q^3$, and $E(q) = 50/q^2$. The expansions we use are

$$\begin{aligned} D(q) &= \frac{\theta_1^d}{q} + \frac{\theta_2^d}{q^2} + \frac{\theta_3^d}{q^3}, \\ R(q) &= \theta_1^r q + \theta_2^r q^2 + \theta_3^r q^3 + \theta_4^r q^4 + \theta_5^r q^5, \\ H(q) &= \theta_1^h q + \theta_2^h q^2 + \theta_3^h q^3 + \theta_4^h q^4 + \theta_5^h q^5, \\ E(q) &= \frac{\theta_1^e}{q} + \frac{\theta_2^e}{q^2} + \frac{\theta_3^e}{q^3}. \end{aligned} \tag{34}$$

With these expansions, we expect to learn $\boldsymbol{\theta}^d = (0, 50, 0)^\top$, $\boldsymbol{\theta}^r = (0.15, -0.01, 0, 0, 0)^\top$, $\boldsymbol{\theta}^h = (0, 2, -0.4, 0, 0)^\top$, and $\boldsymbol{\theta}^e = (0, 50, 0)^\top$. We average the data over 1000 realisations. For saving the solution, the time intervals we use are $I^d = [0, 0.1]$, $I^e = [0, 5]$, $I^h = [5, 10]$, and $I^r = [10, 50]$, with 25, 50, 100, and 250 time points inside each time interval for saving. For interpolating the solution to obtain the averages, we use $n_k = 25$, $n_k = 50$, $n_k = 100$, and $n_k = 50$ over I^d , I^e , I^h , and I^r , respectively.

To now learn the mechanisms, we apply the sequential procedure described for learning them one at a time. For each problem, we apply pruning so that points outside of the 10% and 90% density quantiles or the 20% and 80% velocity quantiles are not included. We find that $\boldsymbol{\theta}^d = (0, 49.60, 0)^\top$, $\boldsymbol{\theta}^e = (0, 49.70, 0)^\top$, $\boldsymbol{\theta}^h = (-0.0084, 0, 0, -0.0011, 0)^\top$, and $\boldsymbol{\theta}^r = (0.15, -0.010, 0, 0, 0)^\top$. The results with all these learned mechanisms are shown in Figure 10. We see from the comparisons in Figure 10(a)–(b) that the PDE results from the learned mechanisms are nearly indistinguishable from the discrete densities. Similar to Case Study 2, $H(q)$ only matches the continuum limit at $q(L(t), t)$. Note also that the solutions in Figure 10(a) go up to $t = 100$, despite the stepwise procedure considering only times up to $t = 50$.

4.6 Inaccurate continuum limit

We now consider data from Figure 3(b) where the continuum limit is inaccurate. Here, $k = 1/5$ and the continuum limit vectors are $\boldsymbol{\theta}^d = (0, 0.2, 0)^\top$, $\boldsymbol{\theta}^r = (0.15, -0.01, 0, 0, 0)^\top$, $\boldsymbol{\theta}^h = (0, 2, -0.4, 0, 0)^\top$, and $\boldsymbol{\theta}^e = (0, 0.2, 0)^\top$. Using the same procedures and expansions as Figure 10, we average the data over 1000 realisations. The time intervals we use are $I^d = [0, 2]$, $I^e = [2, 10]$, $I^h = [10, 20]$, and $I^r = [20, 50]$, using 20 time points for I^d and 200 time points for I^e , I^h , and I^r . We use $n_k = 50$ knots for averaging the solution over I^d , and $n_k = 100$ knots for averaging the solution over I^e , I^h , and I^r .

To apply the equation learning procedure we prune all matrices so that points outside of the 40% and 60% temporal quantiles are eliminated, where the *temporal quantiles* are the quantiles of $\partial q/\partial t$ from the averaged discrete data, and similarly for points outside of the 40% and 60% velocity quantiles. We find $\boldsymbol{\theta}^d = (0, 0.21, 0)^\top$, $\boldsymbol{\theta}^e = (0, 0.23, 0)^\top$, $\boldsymbol{\theta}^h = (-0.15, 0, 0, -0.0079, 0)^\top$, and $\boldsymbol{\theta}^r = (0.11, -0.0067, 0, 0, 0)^\top$. Interestingly, here we learn $R(q)$ is quadratic with coefficients that differ from the continuum limit. The results with all these learned mechanisms are shown in Figure 11. We see from the comparisons in Figure 11 that the PDE results from the learned mechanisms are visually indistinguishable from the discrete densities. Moreover, as in Figure 10, the learned $H(q)$ and $E(q)$ match the continuum results at $q(L(t), t)$ which confirms that the learned continuum limit conserves mass, as expected. Note also that the solutions in Figure 11(a) go up to $t = 250$, despite the stepwise procedure considering only times up to $t = 50$, demonstrating the extrapolation power of our method.

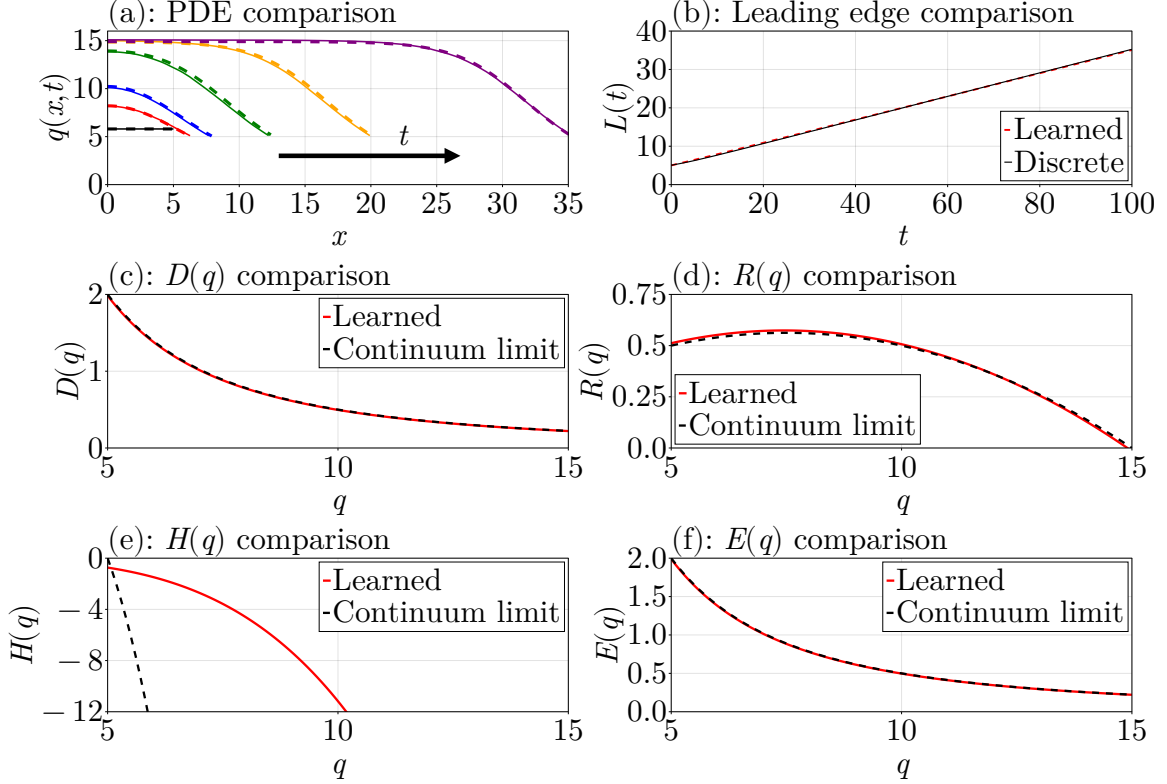


Figure 10: Stepwise equation learning results for Case Study 4: Free boundaries with proliferation, when the continuum limit is accurate, using the learned mechanisms with $\theta^d = (0, 49.60, 0)^\top$, $\theta^e = (0, 49.70, 0)^\top$, $\theta^h = (-0.0084, 0, 0, -0.0011, 0)^\top$, and $\theta^r = (0.15, -0.010, 0, 0, 0)^\top$. (a) Comparisons of the discrete density profiles (solid curves) with those learned from PDEs with the given θ^d , θ^e , θ^h , and θ^r (dashed curves), plotted at the times $t = 0, 5, 10, 25, 50, 100$ in black, red, blue, green, orange, and purple, respectively. The arrow shows the direction of increasing time. (b) As in (a), except comparing the leading edges. (c)–(f) are comparisons of the learned forms of $D(q)$, $R(q)$, $H(q)$, and $E(q)$ with the forms from the continuum limit (8).

5 Conclusion and discussion

In this work, we presented a stepwise equation learning framework for learning continuum descriptions of discrete models describing population biology phenomena. Our approach provides accurate continuum approximations when standard coarse-grained approximations are inaccurate. The framework is simple to implement, efficient, easily parallelisable, and modular, allowing for additional components to be added into a model with minimal changes required to accommodate them into an existing procedure. In contrast to other approaches, like neural networks [41] or linear regression approaches [43], results from our procedure are interpretable in terms of the underlying discrete process. The coefficients incorporated or removed at each stage of our procedure give a sense of the influence each model term contributes to the model, giving a greater interpretation of the results, highlighting an advantage of the stepwise approach over traditional sparse regression methods [32, 37, 38]. The learned continuum descriptions from our procedure enable the discovery of new mechanisms and equations describing the data from the discrete model. For example, the discovered form of $D(q)$ can be interpreted relative to the discrete model, describing the interaction forces between neighbouring cells. In addition, we found in Case Study 4 that, when $k = 1/5$ so that the continuum limit is inaccurate, the positive root of the quadratic form of the source term $R(q)$ is greater than

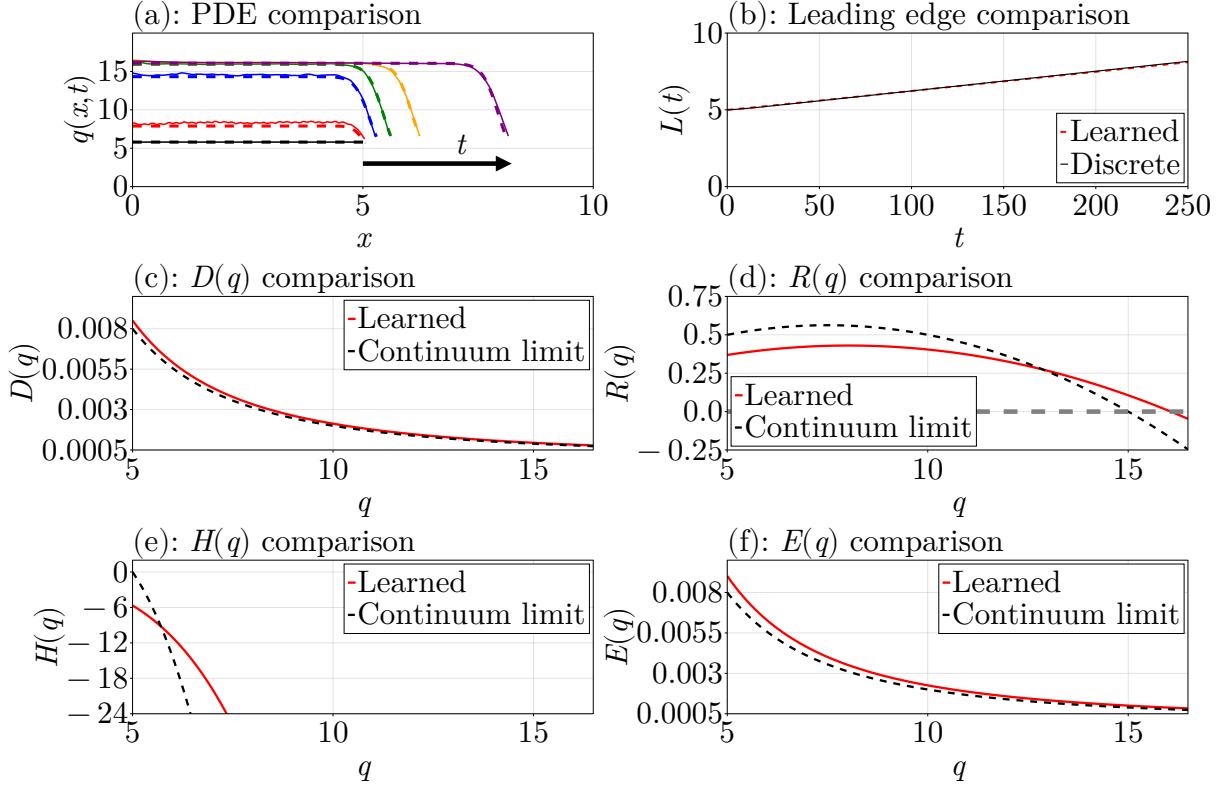


Figure 11: Stepwise equation learning results for Case Study 4: Free boundaries with proliferation, when the continuum limit is inaccurate, using the learned mechanisms with $\theta^d = (0, 0.21, 0)^\top$, $\theta^e = (0, 0.23, 0)^\top$, $\theta^h = (-0.15, 0, 0, -0.0079, 0)^\top$, and $\theta^r = (0.11, -0.0067, 0, 0, 0)^\top$. (a) Comparisons of the discrete density profiles (solid curves) with those learned from PDEs with the given θ^d , θ^e , θ^h , and θ^r (dashed curves), plotted at the times $t = 0, 5, 25, 50, 100, 250$ in black, red, blue, green, orange, and purple, respectively. The arrow shows the direction of increasing time. (b) As in (a), except comparing the leading edges. (c)–(f) are comparisons of the learned forms of $D(q)$, $R(q)$, $H(q)$, and $E(q)$ with the forms from the continuum limit (8).

the mean field carrying capacity density K , as seen in Figure 11. This increase suggests that, when the rate of mechanical relaxation is small relative to the proliferation rates, the mean field carrying capacity density in the continuum description can be different from that in the discrete model.

We demonstrated our approach using a series of four biologically-motivated case studies that incrementally build on each other, studying a discrete individual-based mechanical free boundary model of epithelial cells [10,11,15,16]. In the first two case studies, we demonstrated that we can easily rediscover the continuum limit models derived by Baker et al. [16], including the equations describing the evolution of the free boundary. The last two case studies demonstrate that, when the coarse-grained models are inaccurate, our approach can learn an accurate continuum approximation. The last case study was the most complicated, with four mechanisms needing to be learned, but the modularity of our approach made it simple to apply a sequential procedure to learning the mechanisms, applying the procedure to each mechanism in sequence. Our procedure was able to recover terms that conserved mass, despite not enforcing conservation of mass explicitly. The procedure as we have described does have some limitations, such as assuming that the mechanisms are linear combinations of basis functions, which could be handled more generally by instead using nonlinear least squares [42]. The procedure may also be sensitive to the quality of the data points included in the matrices, and thus to the parameters used for the procedure. In Appendix F, we discuss a parameter sensitivity

study that investigates this in greater detail. In this parameter sensitivity study, we find that the most important parameters to choose are the pruning parameters. These parameters can be easily tuned thanks to the efficiency of our method, modifying each parameter in sequence and using trial and error to determine suitable parameter values.

There are many avenues for future work based on our approach. Firstly, two-dimensional extensions of our discrete model could be considered [55,56], which would follow the same approach except the continuum problems would have to be solved using a more detailed numerical approximation [57–59]. Another avenue for exploration would be to consider applying the discrete model on a curved interface which is more realistic than considering an epithelial sheet on a flat substrate [60,61]. Working with heterogeneous populations of cells, where parameters in the discrete model can vary between individuals in the population, is also another interesting option for future exploration [14]. Uncertainty quantification could also be considered using bootstrapping [42] or Bayesian inference [62]. Allowing for uncertainty quantification would also allow for noisy data sets to be modelled, unlike the idealised, noise-free data used in this work. We emphasise that, regardless of the approach taken for future work, we believe that our flexible stepwise learning framework can form the basis of these potential future studies.

References

- [1] Maclaren OJ, Byrne HM, Fletcher AG, Maini PK. 2015 Models, measurement and inference in epithelial tissue dynamics. *Mathematical Biosciences and Engineering* **12**, 1321–1340.
- [2] Turner S, Sherratt JA, Painter KJ, Savill NJ. 2004 From a discrete to a continuous model of biological cell movement. *Physical Review E* **69**, 021910.
- [3] Alber M, Chen N, Lushnikov PM, Newman SA. 2007 Continuous macroscopic limit of a discrete stochastic model for interaction of living cells. *Physical Review Letters* **99**, 168102.
- [4] Zmurchok C, Bhaskar D, Edelstein-Keshet L. 2018 Coupling mechanical tension and GTPase signaling to generate cell and tissue dynamics. *Physical Biology* **15**, 046004.
- [5] Marée AFM, Grieneisen VA, Edelstein-Keshet L. 2012 How cells integrate complex stimuli: The effect of feedback from phosphoinositides and cell shape on cell polarization and motility. *PLoS Computational Biology* **8**, e1002402.
- [6] Mason J, Jack RL, Bruna M. 2023 Macroscopic behaviour in a two-species exclusion process via the method of matched asymptotics. *Journal of Statistical Physics* **190**.
- [7] Bruna M, Chapman SJ, Schmidtchen M. 2023 Derivation of a macroscopic model for Brownian hard needles. *Proceedings of the Royal Society A: Mathematical, Physical and Engineering Sciences* **479**, 20230076.
- [8] Bruna M, Chapman SJ. 2012a Diffusion of multiple species with excluded-volume effects. *The Journal of Chemical Physics* **137**, 204116.
- [9] Bruna M, Chapman SJ. 2012b Excluded-volume effects in the diffusion of hard spheres. *Physical Review E* **85**, 011103.
- [10] Murray PJ, Edwards CM, Tindall MJ, Maini PK. 2009 From a discrete to a continuum model of cell dynamics in one dimension. *Physical Review E* **80**, 031912.
- [11] Murray PJ, Edwards CM, Tindall MJ, Maini PK. 2012 Classifying general nonlinear force laws in cell-based models via the continuum limit. *Physical Review E* **85**, 021921.
- [12] Tambyah TA, Murphy RJ, Buenzli PR, Simpson MJ. 2021 A free boundary mechanobiological model of epithelial tissues. *Proceedings of the Royal Society A: Mathematical, Physical and Engineering Sciences* **476**, 20200528.

- [13] Murphy RJ, Buenzli PR, Tambyah TA, Thompson EW, Hugo HJ, Baker RE, Simpson MJ. 2021 The role of mechanical interactions in EMT. *Physical Biology* **18**, 046001.
- [14] Murphy RJ, Buenzli PR, Baker RE, Simpson MJ. 2019 A one-dimensional individual-based mechanical model of cell movement in heterogeneous tissues and its coarse-grained approximation. *Proceedings of the Royal Society A: Mathematical, Physical and Engineering Sciences* **475**, 20180838.
- [15] Murphy RJ, Buenzli PR, Baker RE, Simpson MJ. 2020 Mechanical cell competition in heterogeneous epithelial tissues. *Bulletin of Mathematical Biology* **82**, 130.
- [16] Baker RE, Parker A, Simpson MJ. 2019 A free boundary model of epithelial dynamics. *Journal of Theoretical Biology* **481**, 61–74.
- [17] Fozard JA, Byrne HM, Jensen OE, King JR. 2010 Continuum approximations of individual-based models for epithelial monolayers. *Mathematical Medicine and Biology: A Journal of the IMA* **27**, 39–74.
- [18] Supekar R, Song B, Hastewell A, Choi GPT, Mietke A, Dunkel J. 2023 Learning hydrodynamic equations for active matter from particle simulations and experiments. *Proceedings of the National Academy of Sciences of the United States of America* **120**, e2206994120.
- [19] Español P. 2004 Statistical mechanics of coarse-graining. *Novel Methods in Soft Matter Computing* **640**, 69–115.
- [20] Middleton AM, Fleck C, Grima R. 2014 A continuum approximation to an off-lattice individual-cell based model of cell migration and adhesion. *Journal of Theoretical Biology* **359**, 220–232.
- [21] Jeon J, Quaranta V, Cummings PT. 2010 An off-lattice hybrid discrete-continuum model of tumor growth and invasion. *Biophysical Journal* **98**, 37–47.
- [22] Osborne JM, Walker A, Kershaw SK, Mirams GR, Fletcher AG, Pathmanathan P, Gavaghan D, Jensen OE, Maini PK, Byrne HM. 2010 A hybrid approach to multi-scale modelling of cancer. *Philosophical Transactions of the Royal Society A* **368**, 5013–5028.
- [23] Buttenschön A, Edelstein-Keshet L. 2020 Bridging from single to collective cell migration: A review of models and links to experiments. *PLoS Computational Biology* **16**, e1008411.
- [24] Surendran A, Plank MJ, Simpson MJ. 2020 Population dynamics with spatial structure and an Allee effect. *Proceedings of the Royal Society A: Mathematical, Physical and Engineering Sciences* **476**, 20200501.
- [25] Lorenzi T, Murray PJ, Ptashnyk M. 2020 From individual-based mechanical models of multicellular systems to free-boundary problems. *Interfaces and Free Boundaries: Mathematical Analysis, Computation and Applications* **22**, 205–244.
- [26] Romeo N, Hastewell A, Mietke A, Dunkel J. 2021 Learning developmental mode dynamics from single-cell trajectories. *eLife* **10**, e68679.
- [27] Pughe-Sanford JL, Quinn S, Balabanski T, Grigoriev RO. 2023 Computing chaotic time-averages from a small number of periodic orbits. (<https://arxiv.org/abs/2307.09626v1>).
- [28] Vo BN, Drovandi CC, Pettitt AN, Simpson MJ. 2015 Quantifying uncertainty in parameter estimates for stochastic models of collective cell spreading using approximate Bayesian computation. *Mathematical Biosciences* **263**, 133–142.
- [29] Hufton PG, Lin YT, Galla T. 2019 Model reduction methods for population dynamics with fast-switching environments: Reduced master equations, stochastic differential equations, and applications. *Physical Review E* **99**, 032122.

- [30] Ihle T. 2016 Chapman-Enskog expansion for the Vicsek model of self-propelled particles. *Journal of Statistical Mechanics: Theory and Experiment* p. 083205.
- [31] Codling EA, Plank MJ, Benhamou S. 2008 Random walk models in biology. *Journal of the Royal Society Interface* **5**, 813–834.
- [32] Nardini JT, Baker RE, Simpson MJ, Flores KB. 2021 Learning differential equation models from stochastic agent-based model simulations. *Journal of the Royal Society Interface* **18**, 20200987.
- [33] Simpson MJ, Landman KA, Hughes BD. 2010 Cell invasion with proliferation mechanisms motivated by time-lapse data. *Physica A: Statistical Mechanics and its Applications* **389**, 3779–3790.
- [34] Hughes BD. 1995 *Random walks and random environments: Random walks*. Oxford: Clarendon Press.
- [35] Chopard B, Droz M. 1998 *Cellular automata modeling of physical systems*. Cambridge: Cambridge University Press.
- [36] Evans DJ, Morriss G. 2008 *Statistical mechanics of nonequilibrium liquids*. Cambridge: Cambridge University Press.
- [37] Rudy SH, Brunton SL, Proctor JL, Kutz JN. 2017 Data-driven discovery of partial differential equations. *Science Advances* **3**, e1602614.
- [38] Brunton SL, Proctor JL, Kutz JN. 2016 Discovering governing equations from data by sparse identification of nonlinear dynamical systems. *Proceedings of the National Academy of Sciences of the United States of America* **113**, 3932–3937.
- [39] Nardini JT, Lagergren JH, Hawkins-Daarud A, Curtin L, Morris B, Rutter EM, Swanson KR, Flores KB. 2020 Learning equations from biological data with limited time samples. *Bulletin of Mathematical Biology* **82**, 119.
- [40] Lagergren JH, Nardini JT, Lavigne GM, Rutter EM, Flores KB. 2020a Learning partial differential equations for biological transport models from noisy spatio-temporal data. *Proceedings of the Royal Society A: Mathematical, Physical and Engineering Sciences* **476**, 20190800.
- [41] Lagergren JH, Nardini JT, Baker RE, Simpson MJ, Flores KB. 2020b Biologically-informed neural networks guide mechanistic modelling from sparse experimental data. *PLoS Computational Biology* **16**, e1008462.
- [42] VandenHeuvel DJ, Drovandi C, Simpson MJ. 2022 Computationally efficient mechanism discovery for cell invasion with uncertainty quantification. *PLoS Computational Biology* **18**, e1010599.
- [43] Simpson MJ, Baker RE, Buenzli PR, Nicholson R, Maclaren OJ. 2022 Reliable and efficient parameter estimation using approximation continuum limit descriptions of stochastic models. *Journal of Theoretical Biology* **549**, 111201.
- [44] Yamashita T, Yamashita K, Kamimura R. 2007 A stepwise AIC method for variable selection in linear regression. *Communications in Statistics - Theory and Methods* **36**, 2395–2403.
- [45] Guillot C, Lecuit T. 2013 Mechanics of epithelial tissue homeostasis and morphogenesis. *Science* **340**, 1185–1189.
- [46] Bragulla HH, Homberger DG Structure and functions of keratin proteins in simple, stratified, keratinized and cornified epithelia. *Journal of Anatomy* **214**, 516–559.
- [47] Paster I, Stojadinovic O, Yin NC, Ramirez H, Nusbaum AG, Saway A, Patel SB, Khalid L, Isseroff RR, Tomic-Canic M. 2014 Epithelialization in wound healing: A comprehensive review. *Advances in Wound Care* **3**, 445–464.

- [48] Begnaud S, Chen T, Delacour D, Mège RM, Ladoux B. 2016 Mechanics of epithelial tissues during gap closure. *Current Opinion in Cell Biology* **42**, 52–62.
- [49] Paredes J, Figueiredo J, Albergaria A, Oliveira P, Carvalho J, Ribeiro AS, Caldeira J, Costa AM, Simões-Correia J, Oliveira MJ, Pinheiro H, Pinho SS, Mateus R, Reis CA, Leite M, Fernandes MS, Schmitt F, Carneiro F, Figueiredo C, Oliveira C, Seruca R. 2012 Epithelial E- and P-cadherins: Role and clinical significance in cancer. *Biochimica et Biophysica Acta* **1826**, 297–311.
- [50] Hittelman WN. 2006 Genetic instability in epithelial tissues at risk for cancer. *Annals of the New York Academy of Sciences* **952**, 1–12.
- [51] Bezanson J, Edelman A, Karpinski S, Shah VB. 2017 Julia: A fresh approach to numerical computing. *SIAM Review* **59**, 65–98.
- [52] Witelski TP. 1995 Shocks in nonlinear diffusion. *Applied Mathematics Letters* **8**, 27–32.
- [53] Simpson MJ, Landman KA, Hughes BD, Fernando AE. 2010 A model for mesoscale patterns in motile populations. *Physica A: Statistical Mechanics and its Applications* **389**, 1412–1424.
- [54] Johnston ST, Baker RE, McElwain DLS, Simpson MJ. 2017 Co-operation, competition and crowding: A discrete framework linking allee kinetics, nonlinear diffusion, shocks and sharp-fronted travelling waves. *Scientific Reports* **7**, 42134.
- [55] Smith AM, Baker RE, Kay D, Maini PK. 2012 Incorporating chemical signalling factors into cell-based models of growing epithelial tissues. *Journal of Mathematical Biology* **65**, 441–463.
- [56] Osborne JM, Fletcher AG, Pitt-Francis JM, Maini PK, Gavaghan DJ. 2017 Comparing individual-based approaches to modelling the self-organization of multicellular tissues. *PLoS Computational Biology* **13**, e1005387.
- [57] Tam AKY, Simpson MJ. 2023 Pattern formation and front stability for a moving-boundary model of biological invasion and recession. *Physica D: Nonlinear Phenomena* **444**, 133593.
- [58] Sethian JA. 1999 *Level set methods and fast marching methods: evolving interfaces in computational geometry, fluid mechanics, computer vision, and materials science*. Cambridge: Cambridge University Press.
- [59] Macklin P, Lowengrub JS. 2008 A new ghost cell/level set method for moving boundary problems: Application to tumor growth. *Journal of Scientific Computing* **35**, 266–299.
- [60] Morris RG, Rao M. 2019 Active morphogenesis of epithelial monolayers. *Physical Review E* **100**, 022413.
- [61] Chang YW, Cruz-Acuña R, Tennenbaum M, Fragkopoulos AA, García AJ, Fernández-Nieves A. 2022 Quantifying epithelial cell proliferation on curved surfaces. *Frontiers in Physics* **10**.
- [62] Martina-Perez S, Simpson MJ, Baker RE. 2021 Bayesian uncertainty quantification for data-driven equation learning. *Proceedings of the Royal Society A: Mathematical, Physical and Engineering Sciences* **477**, 20210426.
- [63] Versteeg HK, Malalasekera W. 2007 *An introduction to computational fluid mechanics*. Harlow: Prentice Hall 2nd edition.
- [64] Rackauckas C, Nie Q. 2017 DifferentialEquations.jl — A performant and feature-rich ecosystem for solving differential equations in Julia. *Journal of Open Research Software* **5**, 15.
- [65] Hosea ME, Shampine LF. 1996 Analysis and implementation of TR-BDF2. *Applied Numerical Mathematics* **20**, 21–37.

- [66] Davis TA, Palamadai Natarajan E. 2010 Algorithm 907: KLU, A direct sparse solver for circuit simulation problems. *ACM Transactions on Mathematical Software* **37**, 1–17.
- [67] Landau HG. 1950 Heat conduction in a melting solid. *The Quarterly Journal of Mechanics & Applied Mathematics* **8**, 81–94.
- [68] Furzeland RM. 1980 A comparative study of numerical methods for moving boundary problems. *IMA Journal of Applied Mathematics* **26**, 411–429.
- [69] Amemiya T. 1985 *Advanced econometrics*. Cambridge, MA: Harvard University Press.
- [70] Johnson SG. 2010 The NLOpt nonlinear-optimization package. <https://github.com/stevengj/nlopt>. Version 2.7.1.
- [71] Johnson SG. 2013 NLOpt.jl: Package to call the NLOpt nonlinear-optimization library from the Julia language. <https://github.com/JuliaOpt/NLOpt.jl>. Version 0.6.5.

Appendix A Confidence bands for inaccurate continuum limits

In the paper, we show in Figure 3 a series of curves for Case Study 3 and Case Study 4 with $k = 1/5$, finding that the solution to the continuum limit is no longer a good match to the data from the discrete model. Figure 12 shows the confidence bands around each of these curves, showing how the uncertainty evolves over time.

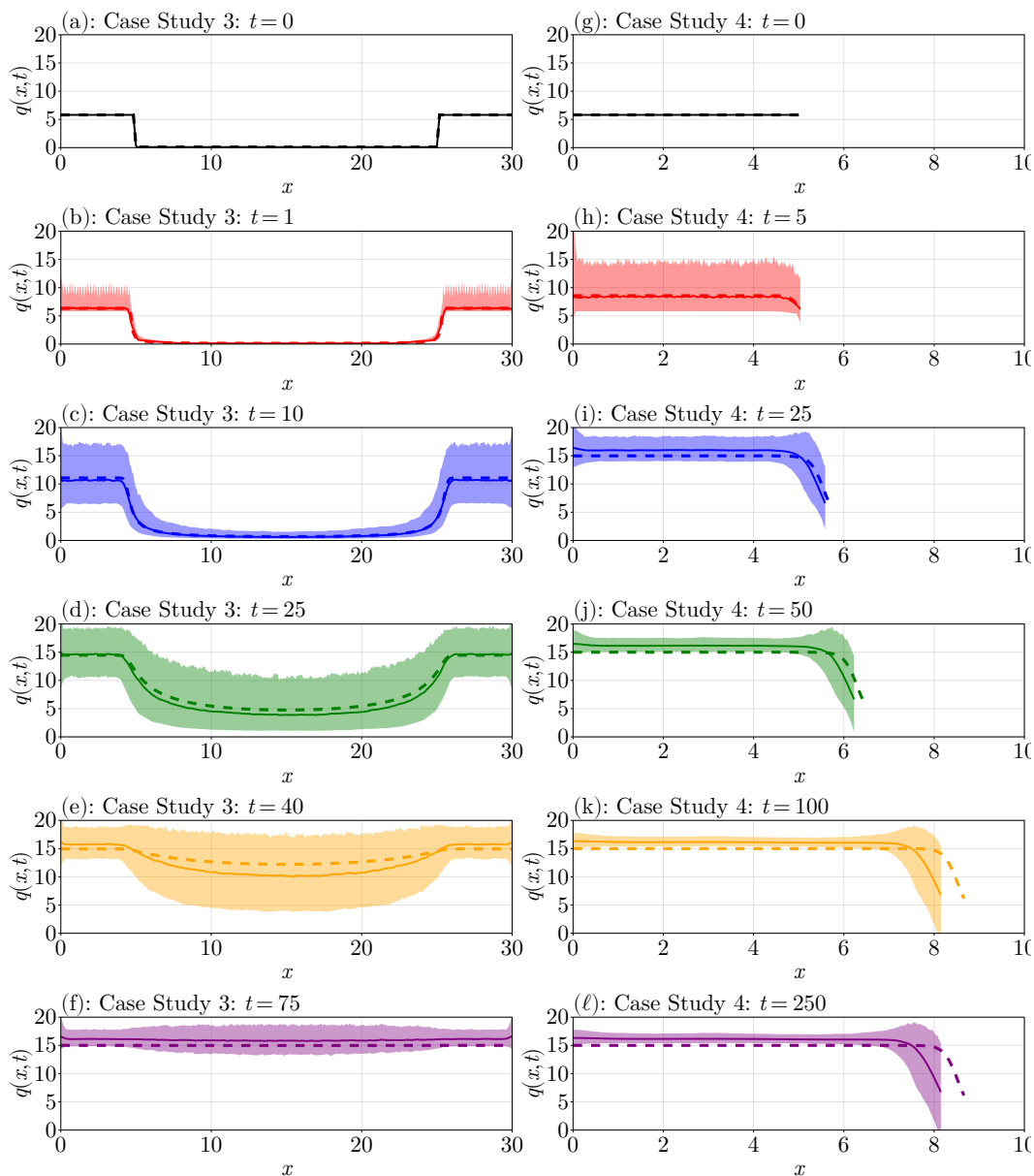


Figure 12: Complementary figure to Figure 3 in the main document, showing inaccurate continuum limits for Case Study 3 (left column) and Case Study 4 (right column). The solid curves are the discrete densities from Equation 2.4 and the dashed curves are solutions to the continuum limit problem in Equation 2.6. The shaded regions show 95% confidence bands from the mean discrete curves at each time shown.

Appendix B Discrete densities at the boundaries

In the paper, we give the following formulae for computing the cell densities from our discrete model at the boundary:

$$q_1(t) = \frac{2}{x_2(t) - x_1(t)} - \frac{2}{x_3(t) - x_1(t)}, \quad q_n(t) = \frac{2}{x_n(t) - x_{n-1}(t)} - \frac{2}{x_n(t) - x_{n-2}(t)}, \quad (35)$$

noting also that $x_1(t) = 0$ in this work. In this section, we derive the expressions for $q_1(t)$ and $q_n(t)$ and show the need for these complicated expressions over those from Baker et al. [16], namely $q_1(t) = 1/(x_2(t) - x_1(t))$ and $q_n(t) = 1/(x_n(t) - x_{n-1}(t))$, through an example.

B.1 Derivation

We give the derivation for $q_n(t)$ only, as $q_1(t)$ is derived in the same way. We follow the idea from Baker et al. [16], relating the cell index i to the density q according to

$$i(x, t) = 1 + \int_0^x q(y, t) dy.$$

Baker et al. [16] use $1 = n - (n - 1)$ together with this relationship to write

$$1 = \int_{x_{n-1}(t)}^{x_n(t)} q(y, t) dy,$$

and Baker et al. [16] then use a right endpoint rule to approximate $q_n(t)$. If we instead use a trapezoidal rule, then

$$1 = \int_{x_{n-1}(t)}^{x_n(t)} q(y, t) dy \approx \left(\frac{x_n(t) - x_{n-1}(t)}{2} \right) (q_n(t) + q_{n-1}(t)). \quad (36)$$

We use this expression to solve for $q_n(t)$:

$$q_n(t) = \frac{2}{x_n(t) - x_{n-1}(t)} - q_{n-1}(t) = \frac{2}{x_n(t) - x_{n-1}(t)} - \frac{2}{x_n(t) - x_{n-2}(t)},$$

which is exactly the formula in (35). We note that an alternative derivation of this formula is to use linear extrapolation, treating the density $1/(x_n(t) - x_{n-1}(t))$ as if it were placed at the cell midpoint $(x_{n-1}(t) + x_n(t))/2$ rather than $x_n(t)$.

B.2 Motivation

Let us now give the motivation for why we need the modifications to the boundary densities in (35) compared to those given in Baker et al. [16]. Consider a mechanical relaxation problem, starting with 30 equally spaced nodes in $0 \leq x \leq 5$, taking the parameters $k = 50$, $s = 1/5$, $\eta = 1$ and leaving the right boundary free. Let us compare the discrete densities at $t = 2$ to those from the continuum limit, as well as estimates of the gradient $\partial q / \partial x$ at the right boundary.

Figure 13 shows our comparisons. Focusing on the densities at the right boundary of Figure 13(a) gives Figure 13(b), where we can see a clear difference in the slopes of each curve. The curve obtained using the approach of Baker et al. [16], using $q_n(t) = 1/(x_n(t) - x_{n-1}(t))$, has a different slope from the continuum limit, whereas the red curve, using $q_n(t) = 2/(x_n(t) - x_{n-1}(t)) - 2/(x_n(t) - x_{n-2}(t))$, has a slope that is much closer to the slope of the continuum limit model at this point. These issues become more apparent when we try to estimate $\partial q / \partial x$ at the boundary for each time, as we would have to do in our equation learning procedure. Shown in Figure 13(c), we see that the estimates of $\partial q / \partial x$ that use $q_n(t) = 1/(x_n(t) - x_{n-1}(t))$ do not resemble what we expect in the continuum limit, namely $\partial q / \partial x = H(q) = 2q^2(1 - qs)$ (using

$q = q(x_n, t)$, where $q(x, t)$ is the solution from the continuum limit partial differential equation (PDE)). Our new expression for $q_n(t)$ gives estimates for $\partial q/\partial x$ that are much closer to $H(q)$, with $H(q)$ passing directly through the center of these estimates across the entire time domain. Thus, our revised formulae (35) are necessary if we want to obtain accurate estimates for the boundary gradients.

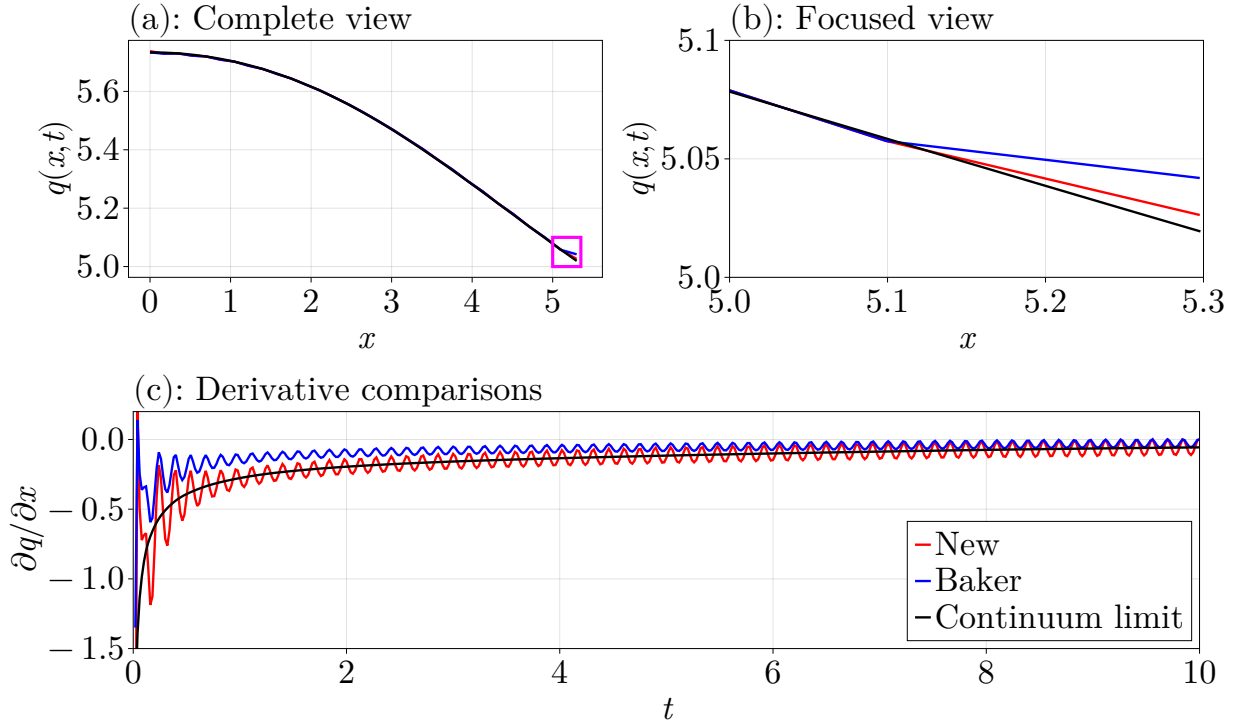


Figure 13: Comparison of the density definitions from Baker et al. [16] to those in (35), using data from a mechanical relaxation problem as an example. (a) Comparing the definitions at $t = 2$ together with densities from the continuum limit PDE. The magenta rectangle shows the region that is zoomed in on in (b). (b) Zooming in on the magenta rectangle from (a) at the right boundary. (c) Comparing estimates of $\partial q/\partial x$ at the right boundary using each definition along with the continuum limit boundary condition $\partial q/\partial x = 2q^2(1 - qs)$.

Appendix C Numerical methods

In this section we give the details involved in solving the PDEs on the fixed and moving domains numerically using the finite volume method [63]. We have provided Julia packages `FiniteVolumeMethod1D.jl` and `MovingBoundaryProblems1D.jl` to implement these methods for the fixed and moving domains, respectively.

C.1 Fixed domain

We start by considering the fixed domain problem. The PDE we consider is

$$\begin{aligned} \frac{\partial q}{\partial t} &= \frac{\partial}{\partial x} \left(D(q) \frac{\partial q}{\partial x} \right) + R(q) & 0 < x < L, t > 0, \\ \frac{\partial q}{\partial x} &= 0 & x \in \{0, L\}, t > 0, \end{aligned} \quad (37)$$

where L is the length of the domain, $D(q)$ is the nonlinear diffusivity function, and $R(q)$ is the source term. To discretise (37), define a grid $0 = x_1 < x_2 < \dots < x_n = L$ with $x_i = (i-1)\Delta x$ and $\Delta x = L/(n-1)$. This grid enables us to define control volumes $\Omega_i = [w_i, e_i]$ for each i , where

$$w_i = \begin{cases} x_1 & i = 1, \\ \frac{1}{2}(x_{i-1} + x_i) & i = 2, \dots, n, \end{cases} \quad \text{and} \quad e_i = \begin{cases} \frac{1}{2}(x_i + x_{i+1}) & i = 1, \dots, n-1, \\ x_n & i = n. \end{cases} \quad (38)$$

The volumes of these control volumes are denoted $V_i = e_i - w_i$, $i = 1, \dots, n$. We then integrate (37) over a single Ω_i to give

$$\frac{d\bar{q}_i}{dt} = \frac{1}{V_i} \left\{ D(q(e_i, t)) \frac{\partial q(e_i, t)}{\partial x} - D(q(w_i, t)) \frac{\partial q(w_i, t)}{\partial x} \right\} + \bar{R}_i, \quad (39)$$

where

$$\bar{q}_i = \frac{1}{V_i} \int_{w_i}^{e_i} q(x, t) dx \quad \text{and} \quad \bar{R}_i = \frac{1}{V_i} \int_{w_i}^{e_i} R[q(x, t)] dx.$$

To proceed, let $q_i = q(x_i, t)$, $D_i = D(q_i)$, $R_i = R(q_i)$ and define the following approximations:

$$\begin{aligned} \bar{q}_i &= q_i & i = 1, \dots, n, \\ \bar{R}_i &= R_i & i = 1, \dots, n, \\ D(q(e_i, t)) &= \frac{1}{2}(D_i + D_{i+1}) & i = 1, \dots, n-1, \\ D(q(w_i, t)) &= \frac{1}{2}(D_{i-1} + D_i) & i = 2, \dots, n, \\ \frac{\partial q(e_i, t)}{\partial x} &= \frac{q_{i+1} - q_i}{\Delta x} & i = 1, \dots, n-1, \\ \frac{\partial q(w_i, t)}{\partial x} &= \frac{q_i - q_{i-1}}{\Delta x} & i = 2, \dots, n. \end{aligned} \quad (40)$$

Using the approximations in (40), (39) becomes

$$\frac{dq_i}{dt} = \frac{1}{V_i} \left[\left(\frac{D_i + D_{i+1}}{2} \right) \left(\frac{q_{i+1} - q_i}{\Delta x} \right) - \left(\frac{D_{i-1} + D_i}{2} \right) \left(\frac{q_i - q_{i-1}}{\Delta x} \right) \right] + R_i, \quad (41)$$

for $i = 2, \dots, n-1$. The boundary conditions at $x = 0$ and $x = L$ are incorporated by simply setting the associated derivative term in (39) to zero, giving

$$\frac{dq_1}{dt} = \frac{1}{2V_1\Delta x} (D_1 + D_2) (q_2 - q_1) + R_1, \quad (42)$$

$$\frac{dq_n}{dt} = -\frac{1}{2V_n\Delta x} (D_{n-1} + D_n) (q_n - q_{n-1}) + R_n. \quad (43)$$

The system of ordinary differential equations (ODEs) is thus given by (41)–(43) and defines the numerical solution to (37). In particular, letting $\mathbf{q}^n = (q_1(t_n), \dots, q_n(t_n))^T$ for some time t_n , we start with $\mathbf{q}^0 = (q_0(x_1), \dots, q_0(x_n))^T$ using the initial condition $q(x, 0) = q_0(x)$, and then integrate forward in time via (41)–(43). This procedure is implemented in the JULIA package `FiniteVolumeMethod1D.jl` which makes use of `DifferentialEquations.jl` to solve the system of ODEs with the `TRBDF2(linsolve = KLUFactorization())` algorithm [64–66].

C.2 Moving boundary problem

We now describe how we solve the PDEs for a moving boundary problem. The PDE we consider is

$$\begin{aligned} \frac{\partial q}{\partial t} &= \frac{\partial}{\partial x} \left(D(q) \frac{\partial q}{\partial x} \right) + R(q) & 0 < x < L(t), t > 0, \\ \frac{\partial q}{\partial x} &= 0 & x = 0, t > 0, \\ \frac{\partial q}{\partial x} &= H(q) & x = L(t), t > 0, \\ q \frac{dL}{dt} &= -E(q) \frac{\partial q}{\partial x} & x = L(t), t > 0. \end{aligned} \tag{44}$$

We assume that $L(t) > 0$ for $t \geq 0$. The discretisation starts by transforming onto a fixed domain using the Landau transform $\xi = x/L(t)$ [16, 67, 68]. With this change of variable, (44) becomes

$$\begin{aligned} \frac{\partial q}{\partial t} &= \frac{\xi}{L} \frac{dL}{dt} \frac{\partial q}{\partial \xi} + \frac{1}{L^2} \frac{\partial}{\partial \xi} \left(D(q) \frac{\partial q}{\partial \xi} \right) + R(q) & 0 < \xi < 1, t > 0, \\ \frac{\partial q}{\partial \xi} &= 0 & \xi = 0, t > 0, \\ \frac{\partial q}{\partial \xi} &= LH(q) & \xi = 1, t > 0, \\ q \frac{dL}{dt} &= -\frac{E(q)}{L} \frac{\partial q}{\partial \xi} & \xi = 1, t > 0. \end{aligned} \tag{45}$$

To now discretise (45), define $\xi_i = (i-1)\Delta\xi$ for $i = 1, \dots, n$, where $\Delta\xi = 1/(n-1)$, and then let

$$w_i = \begin{cases} \xi_1 & i = 1, \\ \frac{1}{2}(\xi_{i-1} + \xi_i) & i = 2, \dots, n, \end{cases} \quad \text{and} \quad e_i = \begin{cases} \frac{1}{2}(\xi_i + \xi_{i+1}) & i = 1, \dots, n-1, \\ \xi_n & i = n. \end{cases} \tag{46}$$

We then define a control volume to be the interval $\Omega_i = [w_i, e_i]$ with volume $V_i = e_i - w_i$, $i = 1, \dots, n$. Next, the PDE in (45) is integrated over this control volume to give

$$\begin{aligned} \int_{w_i}^{e_i} \frac{\partial q}{\partial t} d\xi &= \frac{1}{L} \frac{dL}{dt} \int_{w_i}^{e_i} \xi \frac{\partial q}{\partial \xi} d\xi + \int_{w_i}^{e_i} R(q) d\xi \\ &+ \frac{1}{L^2} \left[D(q(e_i, t)) \frac{\partial q(e_i, t)}{\partial \xi} - D(q(w_i, t)) \frac{\partial q(w_i, t)}{\partial \xi} \right]. \end{aligned} \tag{47}$$

Using integration by parts, the first integral on the right-hand side of (47) is simply

$$\int_{w_i}^{e_i} \xi \frac{\partial q}{\partial \xi} d\xi = e_i q(e_i, t) - w_i q(w_i, t) - \int_{w_i}^{e_i} q d\xi.$$

Next, define the control volume averages

$$\bar{q}_i = \frac{1}{V_i} \int_{w_i}^{e_i} q d\xi, \quad \bar{R}_i = \frac{1}{V_i} \int_{w_i}^{e_i} R d\xi,$$

and set $q_i = q(\xi_i, t)$, $D_i = D(q_i)$, and $R_i = R(q_i)$. With this notation, we define the following set of approximations:

$$\begin{aligned}
\bar{q}_i &= q_i & i &= 1, \dots, n, \\
\bar{R}_i &= R_i & i &= 1, \dots, n, \\
q(e_i, t) &= \frac{1}{2}(q_i + q_{i+1}) & i &= 1, \dots, n-1, \\
q(w_i, t) &= \frac{1}{2}(q_{i-1} + q_i) & i &= 2, \dots, n, \\
D(q(e_i, t)) &= \frac{1}{2}(D_i + D_{i+1}) & i &= 1, \dots, n-1, \\
D(q(w_i, t)) &= \frac{1}{2}(D_{i-1} + D_i) & i &= 2, \dots, n, \\
\frac{\partial q(e_i, t)}{\partial \xi} &= \frac{q_{i+1} - q_i}{\Delta \xi} & i &= 1, \dots, n-1, \\
\frac{\partial q(w_i, t)}{\partial \xi} &= \frac{q_i - q_{i-1}}{\Delta \xi} & i &= 2, \dots, n.
\end{aligned} \tag{48}$$

Using these approximations, (47) becomes

$$\begin{aligned}
\frac{dq_i}{dt} &= \frac{1}{V_i L} \frac{dL}{dt} \left[e_i \left(\frac{q_i + q_{i+1}}{2} \right) - w_i \left(\frac{q_{i-1} + q_i}{2} \right) \right] - \frac{1}{L} \frac{dL}{dt} q_i + R_i \\
&+ \frac{1}{V_i L^2} \left[\left(\frac{D_i + D_{i+1}}{2} \right) \left(\frac{q_{i+1} - q_i}{\Delta \xi} \right) - \left(\frac{D_{i-1} + D_i}{2} \right) \left(\frac{q_i - q_{i-1}}{\Delta \xi} \right) \right].
\end{aligned} \tag{49}$$

The last component to handle are the boundary conditions. Since $\partial q / \partial \xi = 0$ at $\xi = 0$, and since $w_1 = \xi_1 = 0$, our discretisation at $\xi = 0$ becomes

$$\frac{dq_1}{dt} = \frac{1}{V_1 L} \frac{dL}{dt} e_1 \left(\frac{q_1 + q_2}{2} \right) - \frac{1}{L} \frac{dL}{dt} q_1 + R_1 + \frac{1}{V_1 L^2} \left(\frac{D_1 + D_2}{2} \right) \left(\frac{q_2 - q_1}{\Delta \xi} \right). \tag{50}$$

The boundary condition at $\xi = 1$ is $\partial q / \partial \xi = LH(q)$, thus

$$\begin{aligned}
\frac{dq_n}{dt} &= \frac{1}{V_n L} \frac{dL}{dt} \left[q_n - w_n \left(\frac{q_{n-1} + q_n}{2} \right) \right] - \frac{1}{L} \frac{dL}{dt} q_n + R_n \\
&+ \frac{1}{V_n L^2} \left[D_n LH(q_n) - \left(\frac{D_{n-1} + D_n}{2} \right) \left(\frac{q_n - q_{n-1}}{\Delta \xi} \right) \right].
\end{aligned} \tag{51}$$

The remaining boundary condition is the moving boundary condition, $q dL/dt = -[E(q)/L] \partial q / \partial \xi$. Since $\partial q / \partial \xi = LH(q)$, we can write $q_n dL/dt = -[E(q_n)/L] LH(q_n) = -E(q_n)H(q_n)$, giving

$$q_n \frac{dL}{dt} = -E(q_n)H(q_n). \tag{52}$$

The system of ODEs (49)–(52), together with the initial conditions $q_i(0) = q_0(\xi_i L(0))$ for $i = 1, \dots, n$ and $L(0) = L_0$, where $q_0(x)$ and L_0 are the initial conditions, define our complete discretisation. Solving these ODEs over time give values for $q(\xi_i, t_j)$, for some t_j , which gets translated back in terms of x via $x_i = \xi_i L(t_j)$. As in the fixed domain case, we solve these ODEs using `DifferentialEquations.jl` together with the `TRBDF2(linsolve = KLUFactorization())` algorithm [64–66]. We provide our implementation of this procedure in a separate JULIA package, `MovingBoundaryProblems1D.jl`.

Appendix D Additional stepwise equation learning details

In this section, we give some extra details for our stepwise equation learning procedure.

D.1 Discrete mechanism averaging

We start by discussing how we take multiple stochastic realisations from our discrete cell simulations and average them into a single density function.

The discrete simulations give us n_s identically prepared realisations that can be averaged over to estimate the mean density curve. This average can be estimated using a linear interpolant across each time and for each simulation. In particular, let n_k be the number of knots to use for the interpolant at each time. Then, for a given time t_j , let the knots be given by \bar{x}_{ij} for $i = 1, \dots, n_k$. These knots are equally spaced with $\bar{x}_{1j} = 0$ and $\bar{x}_{n_k j} = (1/n_s) \sum_{\ell=1}^{n_s} L_j^{(\ell)}$, where $L_j^{(\ell)}$ is the leading edge at the time t_j from the ℓ th simulation. Then, letting $q^{(\ell)}(x, t_j)$ denote the linear interpolant of the density data at the time t_j from the ℓ th simulation, we define

$$\bar{q}_{ij} = \frac{1}{n_s} \sum_{\ell=1}^{n_s} q^{(\ell)}(\bar{x}_{ij}, t_j), \quad (53)$$

for $i = 1, \dots, n_k$ and $j = 1, \dots, M$. If $q^{(\ell)}(\bar{x}_{ij}, t_j) < 0$ for a given ℓ , then we set $q^{(\ell)}(\bar{x}_{ij}, t_j) = 0$. This density data is used for computing the system (\mathbf{A}, \mathbf{b}) for equation learning when proliferation is involved.

D.2 Derivative estimation

The equation learning system (\mathbf{A}, \mathbf{b}) requires estimates for the derivatives $\partial q_{ij}/\partial t$, $\partial q_{ij}/\partial x$, $\partial^2 q_{ij}/\partial x^2$, and dL_j/dt . To give a formula for an estimate of these derivatives, suppose we have three function values $\{f_1, f_2, f_3\}$ for some function $f(x)$ at the points $\{x_1, x_2, x_3\}$, where $f_i = f(x_i)$ for $i = 1, 2, 3$. These points do not need to be equally spaced. The Lagrange interpolating polynomial through this data is given by

$$g(x) = \frac{(x-x_2)(x-x_3)}{(x_1-x_2)(x_1-x_3)} f_1 + \frac{(x-x_1)(x-x_3)}{(x_2-x_1)(x_2-x_3)} f_2 + \frac{(x-x_1)(x-x_2)}{(x_3-x_1)(x_3-x_2)} f_3,$$

which can be used to estimate the derivatives via $f'(x_i) \approx g'(x_i)$, $i = 1, 2, 3$, and similarly for $f''(x)$. Using this approximation, we write

$$f'(x_1) \approx \left(\frac{1}{x_1-x_2} + \frac{1}{x_1-x_3} \right) f_1 - \frac{x_1-x_3}{(x_1-x_2)(x_2-x_3)} f_2 + \frac{x_1-x_2}{(x_1-x_3)(x_2-x_3)} f_3, \quad (54)$$

$$f'(x_2) \approx \frac{x_2-x_3}{(x_1-x_2)(x_1-x_3)} f_1 + \left(\frac{1}{x_2-x_3} - \frac{1}{x_1-x_2} \right) f_2 + \frac{x_2-x_1}{(x_1-x_3)(x_2-x_3)} f_3, \quad (55)$$

$$f'(x_3) \approx \frac{x_3-x_2}{(x_1-x_2)(x_1-x_3)} f_1 + \frac{x_1-x_3}{(x_1-x_2)(x_2-x_3)} f_2 - \left(\frac{1}{x_1-x_3} + \frac{1}{x_2-x_3} \right) f_3, \quad (56)$$

$$f''(x_i) \approx \frac{2}{(x_1-x_2)(x_1-x_3)} f_1 - \frac{2}{(x_1-x_2)(x_2-x_3)} f_2 + \frac{2}{(x_1-x_3)(x_2-x_3)} f_3, \quad (57)$$

where (57) is valid for $i = 1, 2, 3$.

We can use the formulae (54)–(57) to approximate our required derivatives. For example, taking $\{x_1, x_2, x_3\} = \{t_{j-1}, t_j, t_{j+1}\}$ and $\{f_1, f_2, f_3\} = \{L_{j-1}, L_j, L_{j+1}\}$ gives

$$\frac{dL_j}{dt} \approx \frac{L_{j+1} - L_{j-1}}{h}, \quad j = 2, \dots, M-1, \quad (58)$$

assuming the times are equally spaced with spacing h . The estimate for dL_M/dt is obtained by taking $\{x_1, x_2, x_3\} = \{t_{M-2}, t_{M-1}, t_M\}$ and $\{f_1, f_2, f_3\} = \{L_{M-2}, L_{M-1}, L_M\}$, giving

$$\frac{dL_M}{dt} \approx \frac{3L_M - 4L_{M-1} + L_{M-2}}{2h}. \quad (59)$$

Similarly, taking $\{x_1, x_2, x_3\} = \{x_{i-1,j}, x_{i,j}, x_{i+1,j}\}$ and $\{f_1, f_2, f_3\} = \{q_{i-1,j}, q_{i,j}, q_{i+1,j}\}$ gives

$$\begin{aligned} \frac{\partial^2 q_{ij}}{\partial x^2} &\approx \frac{2}{(x_{i-1,j} - x_{i,j})(x_{i-1,j} - x_{i+1,j})} q_{i-1,j} - \frac{2}{(x_{i-1,j} - x_{i,j})(x_{i,j} - x_{i+1,j})} q_{ij} \\ &+ \frac{2}{(x_{i-1,j} - x_{i+1,j})(x_{i,j} - x_{i+1,j})}, \end{aligned} \quad (60)$$

for $i = 2, \dots, n_j - 1$ and $j = 1, \dots, M$, where n_j is the number of nodes at $t = t_j$. The remaining derivatives can be obtained similarly, ensuring that the appropriate finite difference (backward, central, or forward) is taken for the given point.

The only exception to these rules are for $\partial q / \partial x$ at the boundaries. We find that using simple forward and backward differences there gives better results than with (54) and (55), so we use

$$\frac{\partial q_{1j}}{\partial x} \approx \frac{q_{2j} - q_{1j}}{x_{2j} - x_{1j}}, \quad \frac{\partial q_{n_j j}}{\partial x} \approx \frac{q_{n_j j} - q_{n_j - 1, j}}{x_{n_j j} - x_{n_j - 1, j}}. \quad (61)$$

D.3 Matrix pruning

We now discuss our approach to *matrix pruning*, wherein we discard points from our equation learning matrix \mathbf{A} that do not help to improve our estimates for $\boldsymbol{\theta}$. The approach we take is inspired from the data thresholding idea from VandenHeuvel et al. [42].

To start with our approach, let $\mathbf{q} = (q_{12}, \dots, q_{n_M M})^\top$ be the vector of all discrete densities, letting n_j be the number of nodes at the time $t = t_j$, excluding the densities from the initial condition. Then, take the *threshold tolerance* $0 \leq \tau_q < 1/2$ and compute the interval $(\mathcal{Q}_{\tau_q}^{\mathbf{q}}, \mathcal{Q}_{1-\tau_q}^{\mathbf{q}})$, where $\mathcal{Q}_{\tau}^{\mathbf{y}}$ denotes the 100 τ % quantile of the vector \mathbf{y} . With these intervals, we only include a row in the matrix \mathbf{A} from a given point (x_{ij}, t_j) if $\mathcal{Q}_{\tau_q}^{\mathbf{q}} \leq q_{ij} \leq \mathcal{Q}_{1-\tau_q}^{\mathbf{q}}$.

By choosing the threshold τ_q appropriately, we can significantly improve the estimates for $\boldsymbol{\theta}$ as we only include the most relevant data for estimation, excluding all points with relatively low or high density. Similar thresholds can be defined for the other quantities $|\partial \mathbf{q} / \partial x|$, $|\partial^2 \mathbf{q} / \partial x^2|$, $|\partial \mathbf{q} / \partial t|$, and $|\mathrm{d}\mathbf{L} / \mathrm{d}t|$, defining these vectors similarly to \mathbf{q} , for example $|\partial_t \mathbf{q}| = (|\partial_t q_{12}|, \dots, |\partial_t q_{n_M M}|)^\top$, with respective threshold tolerances $0 \leq \tau_{\partial q / \partial x}, \tau_{\partial^2 q / \partial x^2}, \tau_{\partial q / \partial t}, \tau_{\mathrm{d}L / \mathrm{d}t} < 1/2$.

Appendix E Additional examples

In this section, we give some additional case studies to further demonstrate our method, exploring different force law and proliferation laws, and enforcing conservation of mass together with a discussion about enforcing equality constraints in general.

E.1 Enforcing conservation of mass

In the paper, we discussed at the end of Case Study 2 that it could be possible to enforce mass conservation to fix the issue with $D(q) \neq E(q)$, noting that mass conservation requires $D(q(L(t), t)) = E(q(L(t), t))$. In this section, we consider the results when we fix $D(q) = E(q)$ so that mass is conserved from the outset.

This change $D(q) = E(q)$ is reasonably straightforward to implement in the algorithm, simply replacing the boundary condition (17) so that

$$q(L(t), t) \frac{dL(t)}{dt} = -D(q(L(t), t)) \frac{\partial q(L(t), t)}{\partial x}. \quad (62)$$

This constraint $D(q) = E(q)$ also needs to be reflected in the matrix \mathbf{A} . This is simple to do in this case. Previously, our matrix system took the block diagonal form

$$\begin{bmatrix} \mathbf{A}_1 & \mathbf{0} & \mathbf{0} \\ \mathbf{0} & \mathbf{A}_2 & \mathbf{0} \\ \mathbf{0} & \mathbf{0} & \mathbf{A}_3 \end{bmatrix} \begin{bmatrix} \boldsymbol{\theta}^d \\ \boldsymbol{\theta}^h \\ \boldsymbol{\theta}^e \end{bmatrix} = \begin{bmatrix} \mathbf{b}_1 \\ \mathbf{b}_2 \\ \mathbf{b}_3 \end{bmatrix}. \quad (63)$$

With the constraint $D(q) = E(q)$, (63) becomes

$$\begin{bmatrix} \mathbf{A}_1 & \mathbf{0} \\ \mathbf{0} & \mathbf{A}_2 \\ \mathbf{A}_3 & \mathbf{0} \end{bmatrix} \begin{bmatrix} \boldsymbol{\theta}^d \\ \boldsymbol{\theta}^h \end{bmatrix} = \begin{bmatrix} \mathbf{b}_1 \\ \mathbf{b}_2 \\ \mathbf{b}_3 \end{bmatrix}. \quad (64)$$

We note that, if we wanted to enforce this constraint in Case Study 4, where $\mathbf{A}_1 = [\mathbf{A}^d \ \mathbf{A}^r]$, with \mathbf{A}^d and \mathbf{A}^r defined from (28), then we instead have

$$\begin{bmatrix} \mathbf{A}^d & \mathbf{A}^r & \mathbf{0} \\ \mathbf{0} & \mathbf{0} & \mathbf{A}_2 \\ \mathbf{A}_3 & \mathbf{0} & \mathbf{0} \end{bmatrix} \begin{bmatrix} \boldsymbol{\theta}^d \\ \boldsymbol{\theta}^r \\ \boldsymbol{\theta}^h \end{bmatrix} = \begin{bmatrix} \mathbf{b}_1 \\ \mathbf{b}_2 \\ \mathbf{b}_3 \end{bmatrix}. \quad (65)$$

Let us now consider the results with mass conservation. We use the same parameters that were used to produce the results in Figure 7. In particular, we save the solution at $M = 200$ equally spaced times between $t_1 = 0$ and $t_M = 15$, $\tau_q = 0.35$, $\tau_{dL/dt} = 0.1$, and we start with all coefficients initially inactive. The results we obtain are shown in Table 8 and Figure 14. We see that the form we learn for $D(q)$, and hence for $E(q)$ also, is close to the continuum limit $50/q^2$, and similarly $H(q)$ is a good match; note that $H(q)$ is only evaluated at the boundary densities, which is approximately 5 for $t > 0$, so indeed $H(q)$ matches the continuum limit. Looking to Figure 14(a)–(b), the results are indistinguishable from the continuum limit, which is also what we found in Figure 7 before we enforced conservation of mass.

E.1.1 Imposing linear equality constraints generically

We note that this approach to implementing the constraint $D(q) = E(q)$ requiring such a significant change to the matrix system, giving (64), and to the boundary condition (62), might suggest that the modularity of our approach weakens here. This does not need to be the case, and so let us briefly remark about how constraints such as $D(q) = E(q)$, or any other linear constraints, could be alternatively implemented in our approach seamlessly, further demonstrating the modularity.

Table 8: Stepwise equation learning results for Case Study 2, using the basis expansions (25), saving the results at $M = 200$ equally spaced times between $t_1 = 0$ and $t_M = 15$, pruning with $\tau_q = 0.35$ and $\tau_{dL/dt} = 0.1$, starting with all terms inactive, and enforcing conservation of mass with $D(q) = E(q)$. Coefficients highlighted in blue show the coefficient chosen to be removed or added at the corresponding step.

Step	θ_1^d	θ_2^d	θ_3^d	θ_1^h	θ_2^h	θ_3^h	θ_4^h	θ_5^h	Loss
1	0.000	0.000	0.000	0.000	0.000	0.000	0.000	0.000	-3.371
2	0.000	0.000	0.000	0.000	-0.025	0.000	0.000	0.000	-2.371
3	0.000	47.413	0.000	0.000	-0.025	0.000	0.000	0.000	-1.706
4	0.000	47.413	0.000	0.000	0.443	0.000	0.000	-0.004	-0.688

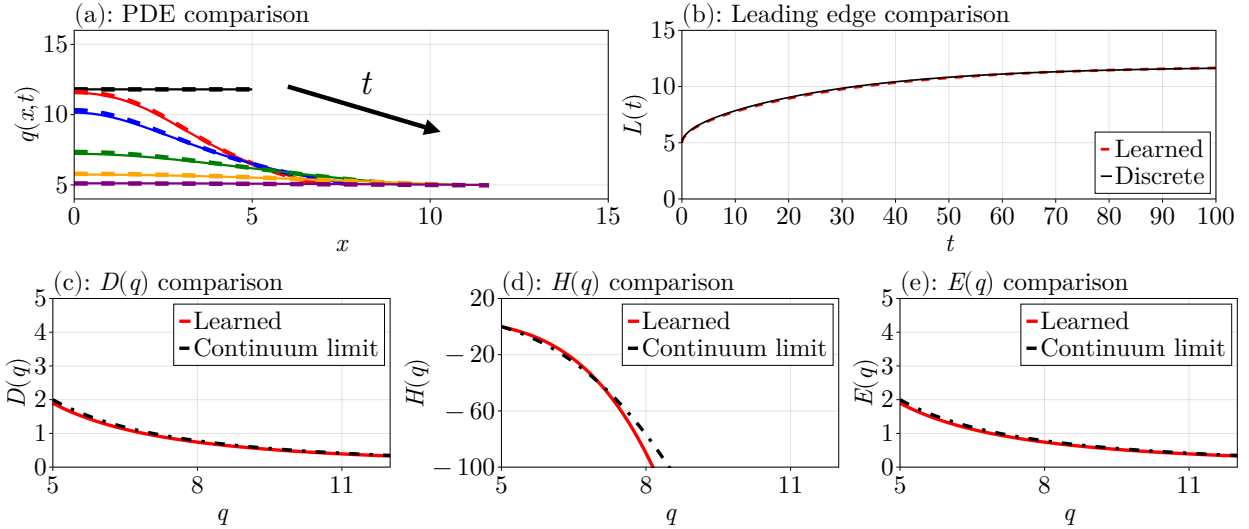


Figure 14: Stepwise equation learning results from Table 8. (a) Comparisons of the discrete density profiles (solid curves) with those from the learned PDE (dashed curves), plotted at the times $t = 0, 5, 10, 25, 50, 100$ in black, red, blue, green, orange, and purple, respectively. (b) As in (a), except comparing the leading edges. (c)–(e) are comparisons of the learned forms of $D(q)$, $H(q)$, and $E(q)$ compared to the forms from the continuum limit.

Suppose we take our system $\mathbf{A}\boldsymbol{\theta} = \mathbf{b}$, with $\mathbf{A} \in \mathbb{R}^{m \times p}$, $\boldsymbol{\theta} \in \mathbb{R}^p$, and $\mathbf{b} \in \mathbb{R}^m$, and suppose we have constraints of the form $\mathbf{Q}^\top \boldsymbol{\theta} = \mathbf{c}$ where $\mathbf{Q} \in \mathbb{R}^{p \times c}$ and $\mathbf{c} \in \mathbb{R}^c$, where $c < p$ and \mathbf{Q} has full rank. The constrained least squares estimator for $\boldsymbol{\theta}$ subject to these constraints, denoted $\hat{\boldsymbol{\theta}}^c$, is then given by

$$\hat{\boldsymbol{\theta}}^c = \hat{\boldsymbol{\theta}} - (\mathbf{A}^\top \mathbf{A})^{-1} \mathbf{Q} \left[\mathbf{Q}^\top (\mathbf{A}^\top \mathbf{A})^{-1} \mathbf{Q} \right]^{-1} (\mathbf{Q}^\top \hat{\boldsymbol{\theta}} - \mathbf{c}), \quad (66)$$

where $\hat{\boldsymbol{\theta}} = (\mathbf{A}^\top \mathbf{A})^{-1} \mathbf{A}^\top \mathbf{b}$ is the unconstrained least squares estimator for $\mathbf{A}\boldsymbol{\theta} = \mathbf{b}$ [69]. Using this formulation, imposing $D(q) = E(q)$ is simple to enforce without changing the boundary condition or the matrix \mathbf{A} ,

simply using $\mathbf{c} = \mathbf{0}_{3 \times 1}$ and

$$\mathbf{Q} = \begin{matrix} \boldsymbol{\theta}^d \\ \boldsymbol{\theta}^h \\ \boldsymbol{\theta}^e \end{matrix} \begin{bmatrix} \mathbf{I}_3 \\ \mathbf{0}_{5 \times 3} \\ -\mathbf{I}_3 \end{bmatrix} = \begin{matrix} \theta_1^d \\ \theta_2^d \\ \theta_3^d \\ \theta_1^h \\ \theta_2^h \\ \theta_3^h \\ \theta_4^h \\ \theta_5^h \\ \theta_1^e \\ \theta_2^e \\ \theta_3^e \end{matrix} \begin{bmatrix} 1 & 0 & 0 \\ 0 & 1 & 0 \\ 0 & 0 & 1 \\ 0 & 0 & 0 \\ 0 & 0 & 0 \\ 0 & 0 & 0 \\ 0 & 0 & 0 \\ 0 & 0 & 0 \\ -1 & 0 & 0 \\ 0 & -1 & 0 \\ 0 & 0 & -1 \end{bmatrix},$$

where \mathbf{I}_n and $\mathbf{0}_{m \times n}$ denote the n -square identity matrix and $m \times n$ zero matrix, respectively. This does not solve the problem entirely, though, since we also have coefficients that we force to zero throughout the stepwise procedure. These zeros constraints can also be imposed by including additional columns of \mathbf{Q} . For example, if θ_1^h and θ_2^d are inactive, then \mathbf{Q} becomes

$$\mathbf{Q} = \begin{matrix} \boldsymbol{\theta}^d \\ \boldsymbol{\theta}^h \\ \boldsymbol{\theta}^e \end{matrix} \begin{bmatrix} \mathbf{I}_3 & \mathbf{e}_2^d & \mathbf{0}_{3 \times 1} \\ \mathbf{0}_{5 \times 3} & \mathbf{0}_{5 \times 1} & \mathbf{e}_1^h \\ -\mathbf{I}_3 & \mathbf{0}_{3 \times 1} & \mathbf{0}_{3 \times 1} \end{bmatrix}, \quad (67)$$

where $\mathbf{e}_2^d = (0, 1, 0)^\top$ and $\mathbf{e}_1^h = (1, 0, 0, 0, 0)^\top$. In particular, each inactive coefficient θ_i corresponds to a new column with a one in the row corresponding to that coefficient. Note that \mathbf{Q} in (67) can be further written as $\mathbf{Q} = [\mathbf{Q}_1 \ \mathbf{Q}_2]$, where \mathbf{Q}_1 are the user-provided constraints $D(q) = E(q)$ and \mathbf{Q}_2 are the constraints imposed by the inactive coefficients, making it easy to incorporate constraints in this manner. Additional care is required to ensure that there are no redundant constraints represented by \mathbf{Q}_1 and \mathbf{Q}_2 as \mathbf{Q} must be full rank. For example, imposing $\theta_1^d = 0$ and $\theta_1^e = 0$ together with the constraint $\theta_1^d = \theta_1^e$ from $D(q) = E(q)$ can be represented using only two constraints rather than three, and the associated matrix

$$\mathbf{Q} = \begin{matrix} \boldsymbol{\theta}^d \\ \boldsymbol{\theta}^h \\ \boldsymbol{\theta}^e \end{matrix} \begin{bmatrix} \mathbf{I}_3 & \mathbf{e}_1^d & \mathbf{0}_{3 \times 1} \\ \mathbf{0}_{5 \times 3} & \mathbf{0}_{5 \times 1} & \mathbf{0}_{5 \times 1} \\ -\mathbf{I}_3 & \mathbf{0}_{3 \times 1} & \mathbf{e}_1^h \end{bmatrix}, \quad (68)$$

where $\mathbf{e}_1^d = (1, 0, 0)^\top$, only has rank 4 rather than the full rank 5. This could be dealt with by finding a basis for the column space of \mathbf{Q} , replacing \mathbf{Q} with the corresponding matrix of basis vectors.

To summarise this discussion, it is straightforward to implement our procedure with the ability to enforce linear equality constraints, allowing for additional constraints, such as conservation of mass, to be enforced. This is easy to code without breaking the modularity of the approach and requiring a significant change to the procedure that would be cumbersome to implement by increasing the complexity of the corresponding code.

E.2 A piecewise proliferation law

In this section, we consider the problem described in Section 3.3 of Murphy et al. [15]. This problem given by Murphy et al. [15] is used to demonstrate a case where the solution of the continuum limit no longer gives a good match with averaged data from the discrete model, as the value of k used is too low relative to the proliferation rate. Here, we show how our method can learn an accurate continuum model in this case.

The example is as follows. We consider $F(\ell_i) = k(s - \ell_i)$ as usual, taking $k = 10^{-4}$ and $s = 0$, but our proliferation law is now given by

$$G(\ell_i) = \begin{cases} 0 & 0 \leq \ell_i < \ell_p, \\ \beta & \ell_i \geq \ell_p, \end{cases} \quad (69)$$

where $\ell_p = 0.2$ is the proliferation threshold and $\beta = 10^{-2}$. We use $\Delta t = 10^{-2}$ for the proliferation events. The initial condition places $n = 41$ equally spaced nodes in $[0, 10]$ so that $\ell_i = 0.25$ at $t = 0$ for each of the 40 cells. In Figure 15, we show a comparison of the discrete data from this problem with the solution of the continuum limit. We also compare the cell numbers $N(t)$, where the cell numbers from the PDE $q(x, t)$ are obtained via $N(t) = \int_0^{10} q(x, t) dx$. We see that the densities from the solution of the continuum limit reach a capacity at 50 cells, while the discrete model instead reaches 80 cells. Note that the densities appear jagged in Figure 13 due to the combination of the averaging procedure from Section D.1 with the variance of the densities for moderate t ; a better averaging method could be to build the knots at each time t based on the node positions themselves, but we do not consider that here as it does not impact the results.

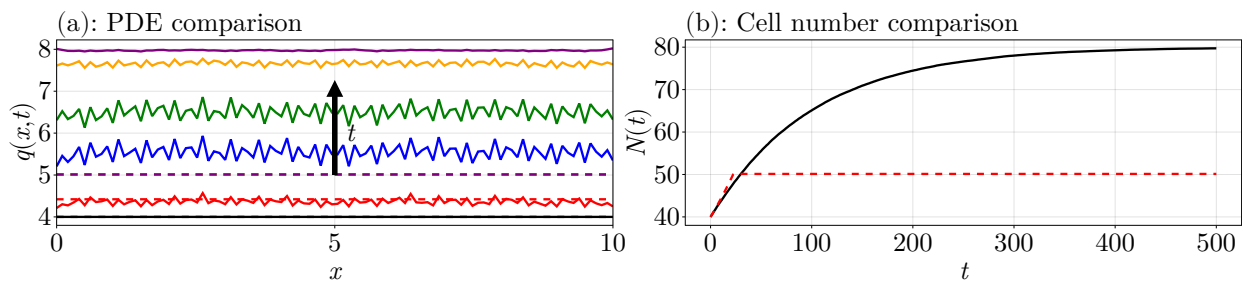


Figure 15: Comparison of the solution of the piecewise proliferation law problem with the solution of continuum limit, where $F(\ell_i) = k(s - \ell_i)$ and $G(\ell_i) = \beta$ for $\ell_i \geq \ell_p$ and $G(\ell_i) = 0$ otherwise, using $k = 10^{-4}$, $s = 0$, $\ell_p = 0.2$, $\eta = 1$, $\beta = 10^{-2}$, and $\Delta t = 10^{-2}$. (a) The solid curves are the discrete densities, and the dashed curves are the densities from the solution of the continuum limit. The arrow shows the direction of increasing time. The density profiles are shown at the times $t = 0, 10, 50, 100, 250, 500$ in black, red, blue, green, orange, and purple, respectively. (b) Comparison of the number of cells from the discrete model with that computed from the solution of the continuum limit, using $N(t) = \int_0^{10} q(x, t) dx$ for the continuum limit case. In (a)–(b), the discrete results are averaged over 1000 identically prepared realisations, using $n_k = 100$ knots for the averaging procedure described in Section D.1.

The continuum limit for this problem is

$$D(q) = \frac{10^{-4}}{q^2} \quad \text{and} \quad R(q) = \begin{cases} 0 & q > 1/\ell_p, \\ 10^{-2}q & q \leq 1/\ell_p. \end{cases}$$

This suggests one possible basis expansion to use for $R(q)$ in our equation learning procedure, with the aim to learn an appropriate continuum approximation to the results in Figure 15, could be

$$R(q) = [\theta_0^r + \theta_1^r q + \theta_2^r q^2 + \theta_3^r q^3] \mathbb{I}\left(q \leq \frac{1}{\ell_p}\right),$$

where $\mathbb{I}(A)$ is the indicator function for the set A . We find that this does not lead to any improved model for this problem, and so we instead consider a polynomial model:

$$R(q) = \theta_0^r + \theta_1^r q + \theta_2^r q^2 + \theta_3^r q^3 + \theta_4^r q^4 + \theta_5^r q^5. \quad (70)$$

For $D(q)$, this mechanism does not appear to be relevant in this example, with the results that follow all giving visually indistinguishable regardless of whether $D(q) = 0$ or $D(q) = 10^{-4}/q^2$. Thus, we do not bother

learning it in this case, simply fixing $D(q) = 10^{-4}/q^2$; if we do not fix $D(q)$, we just end up learning $D(q) = 0$ in the results that follow. With (70) and $D(q) = 10^{-4}/q^2$, the results we obtain are shown in Table 9 and Figure 16.

Step	θ_1^r	θ_2^r	θ_3^r	θ_4^r	θ_5^r	θ_6^r	Loss
1	0.00	0.00	0.00	0.00	0.00	0.00	-1.63
2	0.00	0.00	0.00	0.00	0.00	0.00	-1.53
3	0.077	-0.0096	0.00	0.00	0.00	0.00	-6.22

Table 9: Equation learning results for the piecewise proliferation law problem in Figure 15, fixing $D(q) = 10^{-4}/q^2$ and using the expansion of $R(q)$ in (70). The discrete data is averaged over 1000 identically prepared realisations with $n_k = 100$ knots for interpolating, and the solution is saved every 0.1 units of time between $t = 0$ and $t = 500$.

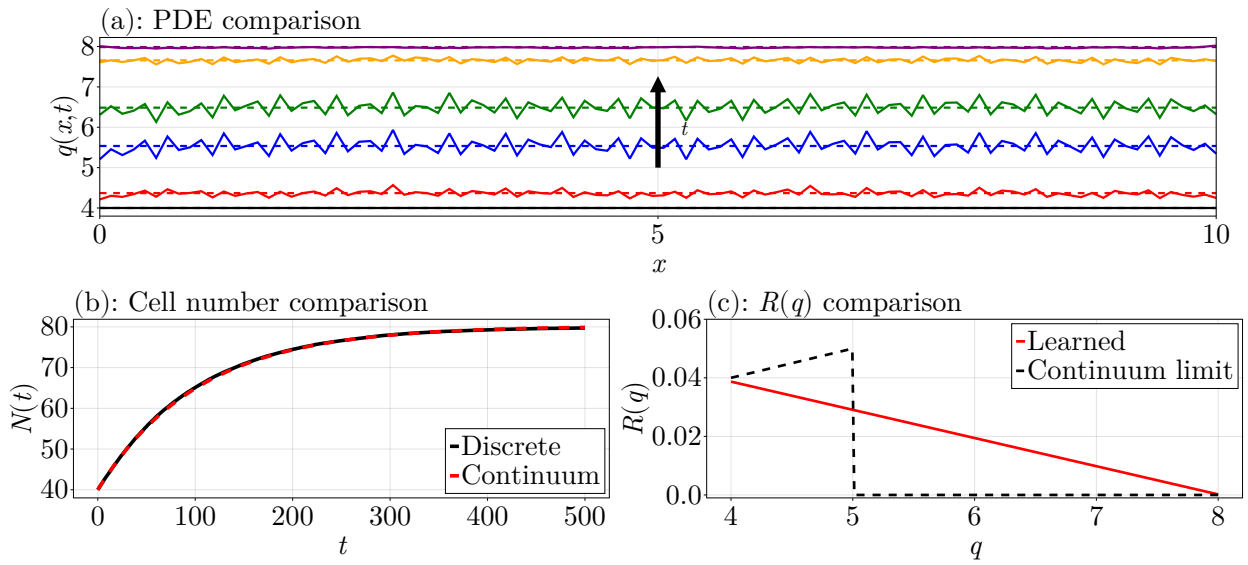


Figure 16: Equation learning results for the piecewise proliferation law problem in Figure 15, using the results from Table 9. (a) Comparison of the averaged discrete densities (solid curves) with the solution of the learned PDE (dashed). The arrow shows the direction of increasing time. The density profiles are shown at the times $t = 0, 10, 50, 100, 250, 500$ in black, red, blue, green, orange, and purple, respectively. (b) Comparison of the cell numbers. (c) Comparison of the learned form of $R(q)$ with the continuum limit form of $R(q)$.

The results in Table 9 and Figure 16 show that we have learned

$$R(q) = 0.077 - 0.0096q. \quad (71)$$

The results in Figure 16(a)–(b) show a good match between the discrete data and the learned PDE solution. Most interestingly, 16(c), we see that this learned $R(q)$ connects the endpoints of the continuum limit form continuously. In particular, $R(q) \approx \beta(K - q) = \beta K(1 - q/K)$, where $K = 8$ is the maximum density from the averaged discrete data. We have thus learned an accurate continuum model to describe this problem, originally from Murphy et al. [15], showing that the piecewise continuum limit form of $R(q)$ is more appropriately described by a simple linear model that connects the jumps in $R(q)$.

E.3 Linear diffusion

In this section, we consider an example where we consider a force law that leads to linear diffusion, namely

$$F(\ell_i) = k \left(\frac{1}{\ell_i} - s \right), \quad (72)$$

We use $k = 20$ and $s = 1$. For the initial condition, we consider a Gaussian initial density $q_0(x)$ with variance three centered at $x = L_0/2$ over $0 \leq x \leq L_0$ with $L_0 = 10$, and scaled so that the initial number of cells is 40, meaning $40 = \int_0^{10} q_0(x) dx$. This leads to

$$q_0(x) = \frac{A}{\sqrt{2\pi\sigma^2}} \exp \left\{ -\frac{1}{2} \left(\frac{x - L_0/2}{\sigma} \right)^2 \right\}, \quad A = \left[\operatorname{erf} \left(\frac{L_0\sqrt{2}}{4\sigma} \right) \right]^{-1} N(0), \quad (73)$$

where $N(0) = 40$, $\sigma^2 = 3$, and erf is the error function. To convert this density into a set of initial cell positions, we consider a set of nodes x_1, \dots, x_{41} with $x_1 = 0$ and $x_{41} = L_0$. The interior nodes $\tilde{\mathbf{x}}(0) = (x_2(0), \dots, x_{40}(0))^T$ are obtained by solving the optimisation problem

$$\tilde{\mathbf{x}}(0) = \operatorname{argmin}_{\tilde{\mathbf{x}} \in \mathbb{R}^{39}} \sum_{i=1}^{41} (q_0(x_i(0)) - q_i)^2$$

subject to the constraint $0 < x_2(0) < \dots < x_{40}(0) < L_0$, where q_i is the density at x_i using our piecewise formulae. This problem is solved using `NLOpt.jl` [70, 71]. The discrete densities we obtain over $0 \leq t \leq 100$ are shown in Figure 17, where we also compare the data to the solution of the continuum limit.

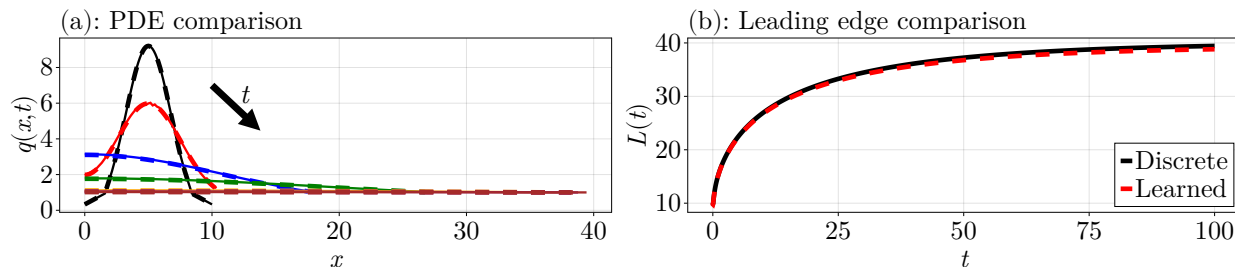


Figure 17: Comparison of the linear diffusion problem with its continuum limit, where $F(\ell_i) = k(a/\ell_i - s)$ with $k = 20$, $s = 1$, $\eta = 1$, and a Gaussian initial density. (a) The solid curves are the discrete densities, and the dashed curves are the densities from the solution of the continuum limit. The arrow shows the direction of increasing time. The density profiles are shown at the times $t = 0, 0.1, 2, 10, 50, 75, 100$ in black, red, blue, green, orange, purple, and brown, respectively. (b) Like in (a), except comparing the leading edges.

To apply the equation learning procedure to this problem, we note that we expect $D(q) = E(q) = 20$, and $H(q) = 2q - 2q^2$. We thus consider

$$\begin{aligned} D(q) &= \frac{\theta_{-2}^d}{q^2} + \frac{\theta_{-1}^d}{q} + \theta_0^d + \theta_1^d q + \theta_2^d q^2, \\ H(q) &= \theta_1^h q + \theta_2^h q^2 + \theta_3^h q^3 + \theta_4^h q^4 + \theta_5^h q^5, \\ E(q) &= \frac{\theta_{-2}^e}{q^2} + \frac{\theta_{-1}^e}{q} + \theta_0^e + \theta_1^e q + \theta_2^e q^2. \end{aligned}$$

Saving the solution between $t = 0$ and $t = 100$ every 0.01 units of time and pruning with $\tau_q = 0.3$ and $\tau_{dL/dt} = 0.2$, we obtain the results in Table 10 and Figure 18, showing a good match between the solution of the learned model and the discrete data.

Step	θ_{-2}^d	θ_{-1}^d	θ_0^d	θ_1^d	θ_2^d	θ_1^h	θ_2^h	θ_3^h	θ_4^h	θ_5^h	θ_{-2}^e	θ_{-1}^e	θ_0^e	θ_1^e	θ_2^e	Loss
1	0.00	0.00	0.00	0.00	0.00	0.00	0.00	0.00	0.00	0.00	0.00	0.00	0.00	0.00	0.00	0.76
2	0.00	0.00	19.18	0.00	0.00	0.00	0.00	0.00	0.00	0.00	0.00	0.00	0.00	0.00	0.00	1.14
3	0.00	0.00	19.18	0.00	0.00	0.00	0.00	0.00	0.00	-0.02	0.00	0.00	0.00	0.00	0.00	0.98
4	0.00	0.00	19.18	0.00	0.00	0.00	0.00	0.00	0.00	-0.02	0.00	0.00	20.05	0.00	0.00	-5.05
5	0.00	0.00	19.18	0.00	0.00	0.00	0.42	0.00	0.00	-0.42	0.00	0.00	20.05	0.00	0.00	-10.73

Table 10: Equation learning results for the linear diffusion problem in Figure 17. The solution is saved every 10^{-2} units of time between $t = 0$ and $t = 100$, and matrix pruning is used with $\tau_q = 0.3$ and $\tau_{dL/dt} = 0.2$.

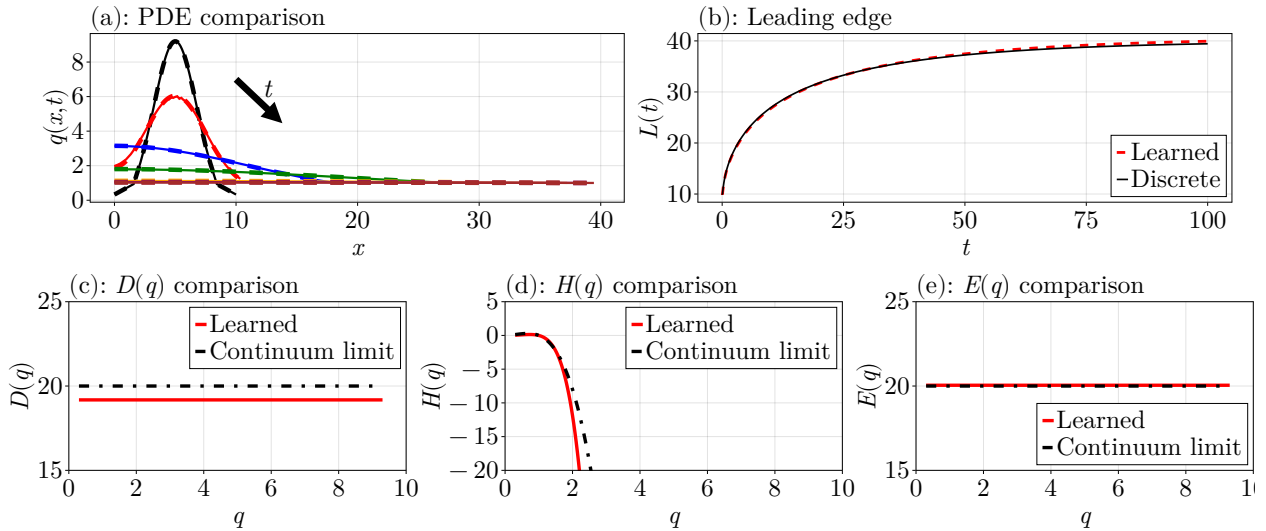


Figure 18: Equation learning results for the linear diffusion problem in Figure 15, using the results from Table 9. (a) Comparison of the discrete densities (solid curves) with the solution of the learned PDE (dashed). The arrow shows the direction of increasing time. The density profiles are shown at the times $t = 0, 0.1, 2, 10, 50, 75, 100$ in black, red, blue, green, orange, purple, and brown, respectively. (b) Line in (a), except comparing the leading edges. (c)–(e) shows comparisons of the learned mechanisms with the forms from the continuum limit.

Appendix F Parameter sensitivity study

In this appendix, we provide a brief parameter sensitivity study, exploring the impact of parameters such as the pruning parameters and the number of time points on the results of our stepwise learning framework. We use Case Study 3 for this purpose, taking the case $k = 1/5$ so that the continuum limit is inaccurate. The parameters we consider are h , the duration between time points; n_s , the number of identically-prepared realisations; t_M , the final time, noting that $t_1 = 0$; n_k , the number of knots used for averaging; and τ_q , the pruning parameter for the density quantiles. We only vary each parameter one at a time, so that the default values for each parameter are $h = 0.1$, $n_s = 1000$, $n_k = 200$, $t_M = 75$, and $\tau_q = 0.25$ while a given parameter is being varied.

To assess the results for each set of parameters we use the loss of the learned model, $\mathcal{L}(\hat{\theta})$. To further examine the results, we divide the results into two categories: those that learn $D(q) = 0$, and those that learn $D(q) \neq 0$. The results of the study are shown in Figure 19. We see that there is little dependence of the results on h , or equivalently on the number of time points. Figure 19(b) shows that n_s needs to be sufficiently large, around $n_s > 500$, in order for any diffusion terms to be selected, although the loss does not change significantly once $D(q)$ terms are identified. The final time is important, where only final times in $50 \leq t_M \leq 75$ give reasonable results. The number of knots is not too important according to Figure 19(d), so long as there are not too many or too few. The most impactful parameter is τ_q , where we need $\tau_q \approx 0.2$ to obtain an adequate learned model; for other case studies which involve other pruning parameters, such as on the derivatives or on the leading edge, we also find that these parameters are the most influential.

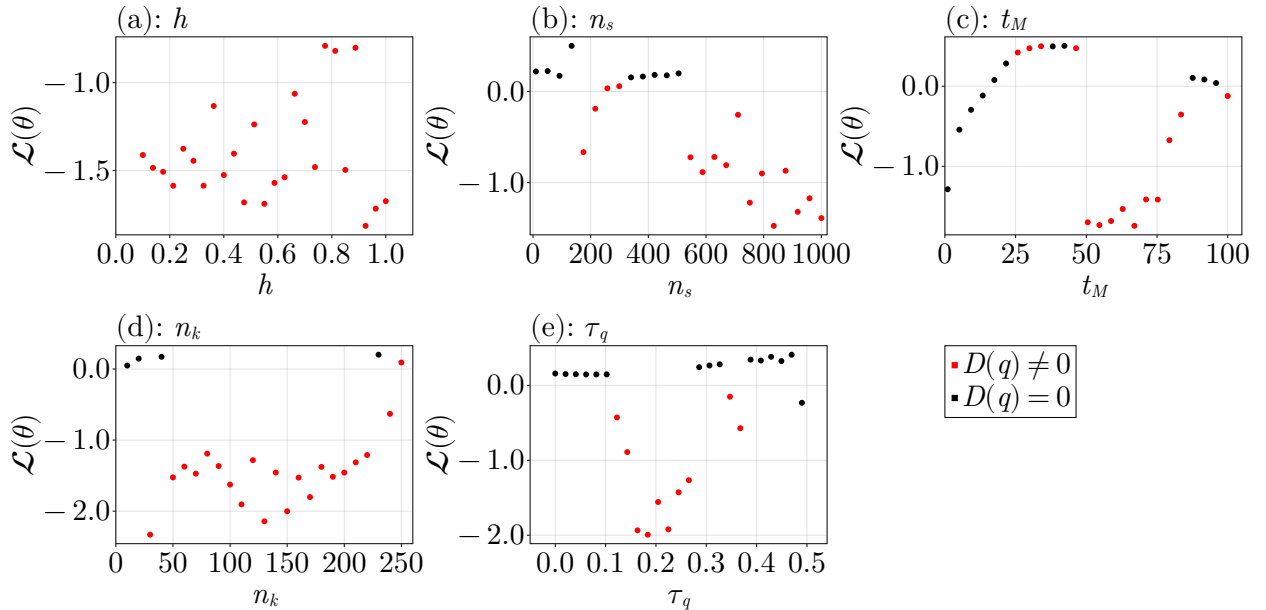


Figure 19: Dependence of $\mathcal{L}(\theta)$, where θ is the vector combined the learned θ^d and θ^r , on the parameters h , n_s , t_M , n_k , and τ_q . For each parameter, as it is varied the other parameters are held at their default values $h = 0.1$, $n_s = 1000$, $t_M = 75$, $n_k = 200$, and $\tau_q = 0.25$.

Overall, Figure 19 shows that τ_q and t_M are the most important parameters for this problem. This is consistent with what we have found for the other case studies, where the choice of pruning parameters is crucial and the time horizon needs to be carefully chosen so that $D(q)$ can be identified. Choosing these parameters can be quite difficult, and trial and error is needed to identify appropriate terms, as well as understanding why a certain model is failing to give good results. For example, in Case Study 2 we determined that we had to shrink the time interval used for learning the results, and that we needed to use

velocity quantiles, by determining what mechanisms are failing to be learned and seeing where the model fails to extrapolate. The values that we used for these parameters, though, had to be chosen with trial and error. Our procedure is efficient enough for this trial and error procedure to be performed quickly, but future work could examine these issues in more detail to simplify the selection of these parameters.